



Two-stage optimization configuration of shared energy storage for multi-distributed photovoltaic clusters in rural distribution networks considering self-consumption and self-sufficiency

Keyi Kang ^{a,b}, Heping Jia ^{a,b,*}, Hongxun Hui ^{c,d}, Dunnan Liu ^{a,b}

^a School of Economics and Management, North China Electric Power University, No. 2 Beinong Road, Beijing 102206, China

^b Beijing Key Laboratory of Renewable Energy and Low-carbon Development, Beijing 102206, China

^c State Key Laboratory of Internet of Things for Smart City, University of Macau, Macao 999078, China

^d Department of Electrical and Computer Engineering, University of Macau, Macao 999078, China

HIGHLIGHTS

- The application value of SES in rural distribution network is studied.
- A cooperative operation strategy for multi-DPV clusters and SES is proposed.
- A two-stage SES configuration model is constructed.
- The synergistic effect of SES and DR is analyzed.

ARTICLE INFO

Keywords:

Rural distribution networks
Self-consumption and self-sufficiency
Shared energy storage
Optimization configuration
Demand response
Levelized annual costs

ABSTRACT

The integration of energy storage (ES) systems with distributed photovoltaic (DPV) generation in rural Chinese distribution networks enhances self-consumption while mitigating grid congestion. However, the geographically dispersed nature of rural DPV deployment leads to suboptimal storage utilization when configuring ES for individual village-level DPV clusters, primarily due to the absence of inter-cluster energy exchange. This operational inefficiency significantly escalates both initial investment and maintenance costs. In this paper, considering the complementarity between outputs of DPV clusters and residential loads in different villages, a cooperative operation strategy for multi-DPV clusters and shared energy storage (SES) is proposed with the goal of improving the self-consumption and self-sufficiency. Then, a comprehensive life-cycle cost-income analysis framework and a two-stage SES optimization configuration model is developed. The proposed model is solved by the particle swarm algorithm with improved adaptive inertia weights (APSO). A rural DPV demonstration zone in northern China serves as the case study, where multiple scenarios incorporating various ES configurations and demand response (DR) implementations are designed. Comparative analysis reveals that SES outperforms distributed energy storage (DES), boosting PV self-consumption by 2.44 %, increasing power self-sufficiency by 2.26 %, and lowering levelized annual costs per rural household by 2.54 %. When integrated with DR, these benefits increase to 3.46 %, 3.20 %, and 3.72 % respectively. The research outcomes provide useful reference for investment planning and coordinated operation of multi-DPV clusters and shared storage systems, facilitating sustainable development of DPV in rural areas.

1. Introduction

In recent years, distributed photovoltaic (DPV) systems in China have achieved significant leapfrog development, playing a pivotal role in ensuring reliable power supply, accelerating the green energy

transition, and fostering rural income growth and employment opportunities [1–2]. By the end of 2024, the cumulative installed capacity of DPV systems reached 370 GW, with an annual power generation of 346.2 TWh, representing 41 % of the total PV power generation [3]. China's abundant and underutilized rooftop resources in rural areas offer a solid foundation for the deployment and development of DPV

* Corresponding author at: School of Economics and Management, North China Electric Power University, No. 2 Beinong Road, Beijing 102206, China.
E-mail address: jiaheping@ncepu.edu.cn (H. Jia).

Nomenclature		
$C_{con,n}^{pv}$	Construction cost of the DPV cluster in the n^{th} village (CNY)	$E_{dis,t}^{es}$
$C_{inv,n,h}^{pv}$	Equipment investment of the DPV cluster for the h^{th} household in the n^{th} village (CNY)	$E_{cha,t}^{es}$
$C_{ins,n,h}^{pv}$	Installation cost of the DPV cluster for the h^{th} household in the n^{th} village (CNY)	$\lambda_{sub,t}^{es}$
H	Total number of households installing the DPV system	R_{res}
$C_{u,inv}$	Unit capacity cost of the DPV system (CNY/kW)	γ
$P_{rat,n,h}^{pv}$	Rated capacity of the DPV system of h^{th} household in the n^{th} village (kWh)	y_t
δ_1	Ratio of installation cost to equipment investment of the DPV system (%)	\hat{y}_t
$C_{mai,n}^{pv}$	Operation and maintenance cost of the DPV system in n^{th} village (CNY)	I
δ_2	Ratio of operation and maintenance cost to construction cost of the DPV system (%)	$h_k^{(l)}$
C_{con}^{es}	Construction cost of the ES system (CNY)	s
C_{inv}^{es}	Equipment investment of the ES system (CNY)	$ReLU$
C_{ins}^{es}	Installation cost of the ES system (CNY)	$F_{bas,t}^{load}$
$C_{u,cap}^{es}$	Unit capacity cost of the ES system (CNY/kWh)	$F_{bas,k,t}^{load}$
$C_{u,pow}^{es}$	Unit power cost of the ES system (CNY/kW)	Ω
Q_{cap}^{es}	Rated capacity of the ES system (kWh)	∂
E_{pow}^{es}	Rated power of the ES system (kW)	$F_{adj,t}^{load}$
$C_{u,ins}^{es}$	Unit capacity installation cost of the ES system (CNY/kWh)	$F_{adj,k,j,t}^{load}$
C_{mai}^{es}	Operation and maintenance cost of the ES system (CNY)	τ_t
δ_3	Operation and maintenance cost rate of the ES system (%)	t_t
C_{rep}^{es}	Battery and equipment replacement cost of the ES system (CNY)	Δt_t
$C_{pur,m}^{es}$	Purchase cost of the m^{th} placement component (CNY)	$t_{t,start,0}$
$C_{rem,m}^{es}$	Installation and removal cost of the m^{th} replacement component (CNY)	$t_{t,start,1}$
B	Replacement frequency of the m^{th} component during the project lifecycle	M
M	Number of the components needing replacement	i
$C_{pur,n}^{grid}$	Annual power purchase cost of the n^{th} village from the power grid (CNY)	W_1
$p_{pur,t}^{grid}$	Electricity price of the power grid in the t^{th} period (CNY/kWh)	U
$E_{pur,n,t}^{grid}$	Electricity purchased by the n^{th} village from the power grid in the t^{th} period (kWh)	Z
$R_{grid,n}^{pv}$	Annual PV grid-connected income of the n^{th} village (CNY)	ζ
$E_{on,n,t}^{pv}$	PV grid-connected electricity of the n^{th} village in the t^{th} period (kWh)	W_2
$p_{on,t}^{pv}$	PV feed-in tariffs of the n^{th} village in the t^{th} period (CNY/kWh)	$E_{dem,t}^{load}$
$E_{gen,n,t}^{pv}$	PV generation of the n^{th} village in the t^{th} period (kWh)	α_t
$E_{sel,n,t}^{pv}$	Electricity of PV self-generation and self-consumption of the n^{th} village in the t^{th} period (kWh)	$L_{rigid,t}^0$
$E_{com,n,t}^{pv}$	PV power supplied to surrounding villages from the n^{th} village in the t^{th} period (kWh)	$L_{flex,t}^0$
$E_{cha,n,t}^{es}$	The charging amount of the n^{th} village to the SES system in the t^{th} period (kWh)	p_t
$E_{dis,n,t}^{es}$	The discharge amount of the SES system to the n^{th} village in the t^{th} period (kWh)	p_0
$R_{sub,n}^{pv}$	Initial installation subsidy income of the DPV cluster in the n^{th} village (CNY/kWh)	Q_t^{es}
$\lambda_{inv,sub}^{pv}$	Unit capacity subsidy price of the DPV cluster (CNY/kW)	SOC_{\max}
R_{sub}^{es}	Annual subsidy income of the ES system (CNY)	Q_{t-1}^{es}
		ϖ_{cha}
		ϖ_{dis}
		ϕ_{\min}
		ϕ_{\max}
		G

w_g^d	Inertia weight of particle q after the d th iteration	t	Hour
w_{\min}	Predefined minimum inertia coefficients	u	Year
w_{\max}	Predefined maximum inertia coefficients	$L_{total,t}$	Total load at time t (kW)
$f(x_q^d)$	Fitness value of particle q at the d th iteration	Δp_0	Electricity price variation, $\Delta p_0 = p_t - p_0$
$f_{average}^d$	Average fitness value of particle q at the d th iteration	e_{tk}	Price elasticity coefficient of rigid load at time t to price at time k
f_{\min}^d	Minimum fitness value of particle q at the d th iteration	η_{tk}	Price elasticity coefficient of flexible load at time t to price at time k
N	Number of villages in rural distribution network		
T	Number of time periods including t in a year		

systems. Driven by the ‘county-wide DPV promotion’ initiative, rooftop PV deployment in rural areas is rapidly expanding [4]. As of September 2024, the installed capacity of DPV systems in rural China has reached 150 GW, and the cumulative number of installed households has exceeded 6 million, contributing an average annual income of 11 billion CNY to farmers [5].

The inherent intermittency and volatility characteristics of PV power generation pose significant challenges to modern power systems [6–7]. The rapid expansion of DPV capacity is progressively saturating the integration potential of 110 kV and sub-110 kV distribution networks, leading to widespread PV curtailment in regions with insufficient grid hosting capacity [8]. Concurrently, the increasing penetration of DPV systems has exacerbated grid stability challenges, including transformer reverse power flow overloads and voltage violations, posing significant threats to distribution network security [9–10]. The adoption of on-site consumption and ES technologies has emerged as a critical solution, enabling the direct utilization or storage of energy at or near the generation site. This approach reduces reliance on long-distance transmission networks while enhancing PV self-consumption and self-sufficiency [11–13].

The academic community is actively seeking solutions to enhance PV self-consumption and building self-sufficiency [14–18]. Jiang et al. [19] developed a time-of-use (TOU) optimization model based on park users’ power consumption patterns, leveraging differentiated tariff packages to guide load transfer and improve PV self-use. Shao et al. [20] aimed to minimize microgrid power deviations by dynamically optimizing TOU tariffs, thereby enhancing renewable energy self-consumption. However, TOU price optimization is limited to adjustable loads. An alternative approach involves ES systems, which store surplus PV electricity for later use, significantly boosting building self-sufficiency. It should be noted here that PV self-consumption refers to the share of generated power used directly or for storage charging, while self-sufficiency denotes the proportion of total load met by renewable energy or storage discharge. Argyrou et al. [21] introduced a dynamic local PMA algorithm for battery-supercapacitor hybrid storage, markedly improving PV self-consumption. Ahmadihangar et al. [22] designed a multi-objective scheduling method incorporating battery storage to minimize grid purchases and enhance self-sufficiency. Mulleriyawage et al. [23] proposed a demand-side management strategy integrating DPV, residential loads, and storage to reduce power costs and increase self-consumption. Abdalla et al. [24] explored an energy management strategy combining electric vehicles, ES, household loads, and PV to further optimize grid reliance and self-sufficiency. Current research predominantly focuses on urban industrial, commercial, and residential areas. However, rural distribution networks differ significantly from urban ones. They have lower carrying capacity and lower residential electricity loads than industrial and commercial areas [25–26]. These factors exacerbate the spatial and temporal mismatch between DPV generation and load demand in rural areas, making local PV consumption more challenging. Thus, the scientific deployment of ES systems in rural areas is crucial for enhancing PV self-consumption and self-sufficiency.

Addressing the challenge of ES configuration self-consumption of DPV in rural areas, Wang et al. [27] proposes an optimized allocation

method based on an improved particle swarm optimization algorithm. Research indicates that ES can reduce the PV curtailment rate by 37.51 % in off-grid mode and increase local absorption by 29.09 % in grid-connected mode. Wang et al. [28] validated the benefits of ES in enhancing PV consumption through an orderly charging scheduling model and an ES configuration model for electric vehicles. Wang et al. [29] developed a dual-objective capacity planning model aimed at minimizing PV grid-connected power and maximizing system benefits, demonstrating that ES configuration can reduce PV grid-connected power by 38.65 %. However, rural distribution networks in China exhibit extensive geographic dispersion and numerous DPV points. Existing studies largely focus on single-village PV clusters, overlooking inter-village power complementarity, which leads to underutilization of ES and suboptimal investment returns. In contrast, a cross-village SES offers a more cost-effective and technically viable solution by optimizing resource allocation and enhancing power complementarity.

As an innovative approach, SES planning and operation have garnered significant academic interest. Regarding modeling methods, Li et al. [30] developed a master-slave game-based model integrating SES and PV communities, achieving a 17.16 % reduction in power costs through bi-level optimization. Kang et al. [31] proposed a reinforcement learning-based framework for planning community battery ES, demonstrating a 38 % increase in economic profits. Addressing the community ES sharing mechanism, Li et al. [32] formulated a robust optimization model minimizing annual operating costs, yielding a 6.09 % cost reduction. Chang et al. [33] employed mixed-integer linear programming to validate the cost advantages of SES in community settings. For renewable energy integration, the two-tier model by Ma et al. [34] confirmed that SES significantly reduces wind and solar curtailment, generating \$154 million in benefits. Yang et al. [35] showed that SES effectively reduces deviation costs for renewable energy producers and improves grid-connection efficiency. In industrial park applications, the model proposed by Cao et al. [36], based on a reputation factor pricing strategy, proves effective in reducing carbon emissions and lowering costs for industrial users. Despite substantial advancements in SES modeling and optimization, most studies prioritize cost or profit optimization for system operators or investors, with limited focus on the objective renewable energy self-consumption.

Based on the above issues, this study examines the disparities in the installed capacity of DPV across villages and the varying electricity demands of rural residents within the rural distribution network. It proposes a cooperative operation strategy for multi-DPV clusters and SES, focusing on PV self-consumption and self-sufficiency. A two-stage optimization model for SES configuration is developed, considering the dual objectives of rural residents’ leveled annual cost and PV self-consumption. Multiple scenarios are analyzed, considering different ES configurations and the introduction of DR. The comparison evaluates the impact on PV self-consumption and self-sufficiency levels, as well as the cost-benefit status of rural residents under various scenarios. Results demonstrate the positive effects of SES and DR collaboration in enhancing PV self-consumption and reducing costs for rural residents, offering valuable insights for the optimal operation of multi-DPV clusters in rural distribution networks. The main contributions of this paper

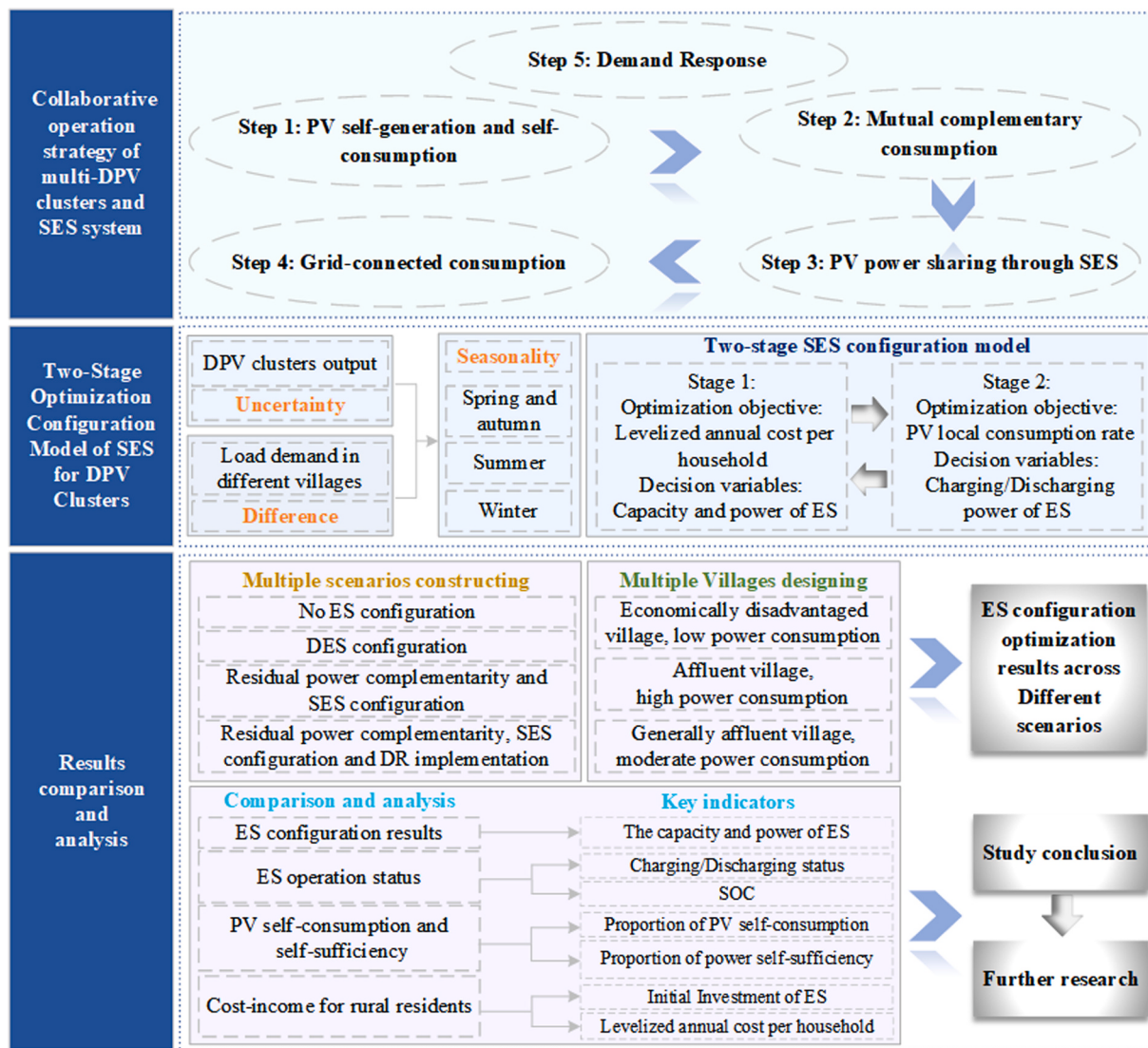


Fig. 1. The research framework of the study.

are as follows:

- (1) Exploiting the complementarity between the output of DPV clusters across different rural villages and residential electricity demand, a collaborative operation strategy involving multi-cluster PV and a SES system is proposed. This approach enhances PV self-consumption and self-sufficiency in rural areas.
- (2) A two-stage optimization model for SES configuration is developed. By examining various storage schemes, the model highlights the benefits of SES in boosting PV self-consumption, reducing grid power dependence, and lowering costs for rural residents, thus providing a basis for rational SES planning.
- (3) The synergistic interaction between SES and DR further enhances PV self-consumption and self-sufficiency, while simultaneously reducing the levelized annual cost for rural residents, improving energy efficiency, and optimizing economic performance.

The structure of the remaining parts of this paper is as follows: Section 2 proposes a cooperative operation strategy for multi-DPV clusters and SES. Section 3 presents a comprehensive life-cycle cost-income analysis framework of the multi-DPV clusters and SES system. Section 4 establishes a PV power generation and residential electricity consumption model, as well as a two-stage SES optimization

configuration model. Section 5 conducts a case analysis using a DPV promotion area within a certain rural distribution network as an example. Finally, Section 6 is the conclusion of this paper. The research framework of this paper is illustrated in Fig. 1.

2. Collaborative operation strategy of multi-DPV clusters and SES system

Given the high penetration of DPV systems in rural distribution networks, which threatens their safe and stable operation, this paper proposes a cooperative operation strategy integrating multi-DPV clusters and SES system. The strategy enhances the PV self-consumption and alleviates grid connection pressure. The key steps are as follows:

Step 1: PV self-generation and self-consumption.

Supply Side: Each village prioritizes self-use of locally generated PV power.

Demand Side: Residents first consume PV electricity produced within their village.

Step 2: Mutual complementary consumption.

Supply Side: Excess PV power is transferred to neighboring villages with insufficient supply.

Demand Side: If local demand exceeds supply, electricity is sourced from villages with surplus PV power.

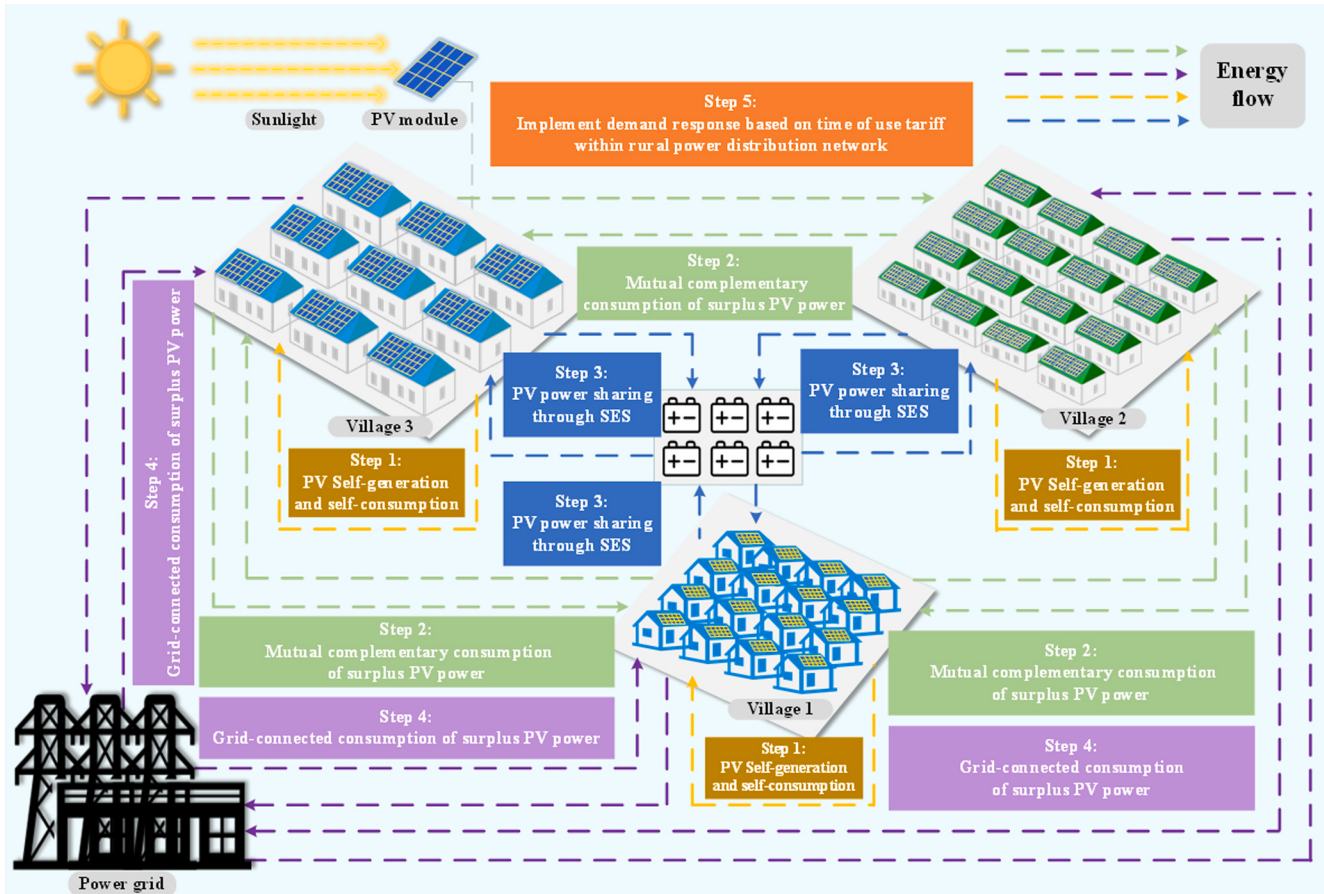


Fig. 2. Collaborative operation strategy of multi-DPV clusters and SES system in rural areas.

Step 3: PV power sharing through SES.

Supply Side: Any remaining surplus is stored in a SES system.

Demand Side: If load demand persists after redistribution, power is drawn from SES.

Step 4: Grid-connected consumption.

Supply Side: Residual PV power is fed into the distribution network.

Demand Side: If load demand remains unmet, power is purchased from the grid.

Step 5: Demand response.

Rural users participate in DR programs, adjusting consumption patterns based on time-of-use pricing to shift peak loads and enhance system efficiency.

The schematic diagram of collaborative operation strategy is shown in Fig. 2.

3. Cost-income analysis framework for multi-DPV clusters and SES system

3.1. Cost analysis for multi-DPV clusters and SES system

(1) Construction cost of DPV.

The construction cost of DPV comprises equipment investment and installation costs. The total construction cost for the n^{th} village DPV cluster is expressed as Eq. (1):

$$C_{con,n}^{pv} = \sum_{h=1}^H \left(C_{inv,n,h}^{pv} + C_{ins,n,h}^{pv} \right) \quad (1)$$

DPV equipment investment is quantified as the product of system rated capacity and unit capacity cost, as formulated in Eq. (2).

Installation costs are typically calculated as a fixed percentage of equipment investment, as demonstrated in Eq. (3):

$$C_{inv,n,h}^{pv} = C_{u,inv} P_{rat,n,h}^{pv} \quad (2)$$

$$C_{ins,n,h}^{pv} = C_{inv,n,h}^{pv} \times \delta_1 \quad (3)$$

(2) Operation and maintenance cost of DPV.

For sub-10 kW systems, operation and maintenance costs are negligible. Larger-scale PV plants require operation and maintenance budgeting at 1–3 % of total investment, as specified in Eq. (4):

$$C_{mai,n}^{pv} = C_{inv,n}^{pv} \times \delta_2 \quad (4)$$

(3) Construction cost of SES.

The construction cost of SES includes both equipment investment and installation costs, calculated as Eq. (5):

$$C_{con}^{es} = C_{inv}^{es} + C_{ins}^{es} \quad (5)$$

Equipment investment consists of capacity-related and power-related costs, formulated in Eq. (6). Installation costs vary with system type and scale, as expressed in Eq. (7):

$$C_{inv}^{es} = C_{u,cap} \times Q_{cap}^{es} + C_{u,pow} \times E_{pow}^{es} \quad (6)$$

$$C_{ins}^{es} = C_{u,ins}^{es} \times Q_{cap}^{es} \quad (7)$$

(4) Operation and maintenance cost of SES.

Operation and maintenance costs encompass routine maintenance, emergency services, charge state management, and energy loss compensation. These are typically calculated as a percentage of initial investment, as shown in Eq. (8):

$$C_{mai}^{es} = C_{inv}^{es} \times \delta_3 \quad (8)$$

(5) Replacement cost of SES.

Given the shorter lifespan of storage systems compared to DPV projects, battery and equipment replacement costs must be considered, calculated as Eq. (9):

$$C_{rep}^{es} = \sum_{m=1}^M (C_{pur,m}^{es} \times B + C_{rem,m}^{es} \times B) \quad (9)$$

(6) Grid electricity procurement cost.

When local generation and storage cannot meet village demand, supplementary electricity is purchased from the grid, calculated as Eq. (10):

$$C_{pur,n}^{grid} = \sum_{t=1}^T E_{pur,n,t}^{grid} \times p_{pur,t}^{grid} \quad (10)$$

3.2. Income analysis for multi-DPV clusters and SES system

(1) DPV grid-connected income.

Grid-connected income is calculated as the product of PV grid-connected power and feed-in tariff. The income calculation is shown in Eq. (11). Under the proposed multi-cluster coordination strategy, each village's grid-connected power equals total PV generation minus self-consumption, inter-village complementary, and storage charging, as shown in Eq. (12):

$$R_{grid,n}^{pv} = \sum_{t=1}^T E_{on,n,t}^{pv} \times p_{on,t}^{pv} \quad (11)$$

$$E_{on,n,t}^{pv} = E_{gen,n,t}^{pv} - E_{sel,n,t}^{pv} - E_{com,n,t}^{pv} - E_{cha,n,t}^{pv} \quad (12)$$

(2) DPV subsidy income.

Governments provide either upfront installation or generation-based subsidies. Given that over 50 % of Chinese regions implement upfront subsidies (based on available statistics), this study adopts the upfront subsidy model, calculated as Eq. (13):

$$R_{sub,n}^{pv} = \sum_{h=1}^H P_{rat,n,h}^{pv} \times \lambda_{inv,sub}^{pv} \quad (13)$$

(3) SES subsidy.

Local governments typically provide time-limited subsidies based on actual discharged power, calculated as Eq. (14):

$$R_{sub}^{es} = \sum_{t=1}^T E_{dis,t}^{es} \times \lambda_{sub}^{es} \quad (14)$$

(4) Fixed asset residual value.

At project termination, recoverable materials from decommissioned assets are valued as original asset value multiplied by residual rate, calculated as Eq. (15):

$$R_{res} = \left(\sum_{n=1}^N C_{con,n}^{pv} + C_{con}^{es} \right) \times \gamma \quad (15)$$

4. Methods

4.1. Prediction model for PV power output

To enhance the accuracy of PV power prediction, this paper proposes a GA-CNN-GRU model incorporating an attention mechanism. The methodology comprises the following steps:

(1) Data preprocessing.

Anomalies and missing values in historical PV data are corrected. The Pauta criterion (3σ principle) is employed to eliminate outliers, while missing data are filled via linear interpolation:

$$x_i = x_{i-1} + \frac{(x_{i+1} - x_{i-1})}{2} \quad (16)$$

(2) Feature selection.

The Pearson Correlation Coefficient quantifies the relationship between meteorological factors and PV output:

$$\rho_{X,Y} = \frac{\text{cov}(X, Y)}{\sigma_X \sigma_Y} \quad (17)$$

where $\text{cov}(X, Y)$ denotes covariance, and σ_x and σ_y represent the standard deviations of variables X and Y , respectively. Features with strong correlations ($|\rho| \geq 0.5$), such as irradiance and humidity, are selected as model inputs.

(3) Genetic algorithm-based weight optimization.

A Genetic Algorithm (GA) optimizes feature weights ω_i by minimizing the prediction error:

$$\min \sum_{t=1}^I y_t - \hat{y}_t \quad (18)$$

where y_t is the actual output, \hat{y}_t is the predicted value, and I is the sample size. Weights are iteratively refined through selection, crossover, and mutation operations.

(4) CNN feature extraction.

One-dimensional convolution extracts local temporal features through the operation:

$$h_k^{(l)} = \text{ReLU} \left(\sum_{i=1}^m \omega_k^{(l)} \times x_{i:i+s-1}^{(l-1)} + b_k^{(l)} \right) \quad (19)$$

where $h_k^{(l)}$ denotes the output of the k -th convolutional kernel at layer l , $\omega_k^{(l)}$ and $b_k^{(l)}$ represent weights and bias respectively, s is the kernel size, and ReLU serves as the activation function.

(5) Attention mechanism.

An attention mechanism dynamically allocates weights to critical timesteps [37]. The attention score α_t is computed as:

$$\alpha_t = \frac{\exp(e_t)}{\sum_{j=1}^T \exp(e_t)}, e_t = \tanh(W_a h_t + b_a) \quad (20)$$

where h_t is the GRU hidden state, while W_a and b_a are trainable parameters.

(6) GRU temporal prediction.

The GRU captures long-term dependencies via update gate z_t and reset gate r_t [38]:

$$\begin{aligned} z_t &= \sigma(W_a \bullet [h_{t-1}, x_t]), r_t = \sigma(W_r \bullet [h_{t-1}, x_t]) \\ \tilde{h}_t &= \tanh(W_h \cdot [r_t \odot h_{t-1}, x_t]), h_t = (1 - z_t) \odot h_{t-1} + z_t \odot \tilde{h}_t \end{aligned} \quad (21)$$

The final prediction output is given by:

$$\hat{y}_t = W_o h_t + b_o \quad (22)$$

where W_o and b_o denote output layer parameters. By combining meteorological features with historical output data, the model achieves higher prediction accuracy.

4.2. Residential DR model based on TOU pricing

Considering the impact of time-of-use (TOU) price policies on residential electricity consumption patterns [39], the total load is partitioned into two distinct categories: price-insensitive rigid loads (e.g., lighting, refrigerators) and price-sensitive flexible loads (e.g., air conditioners, electric vehicles). Separate elasticity response models are established for each category.

(1) Construction of load elasticity matrices.

For rigid loads, which exhibit minimal price responsiveness, their elasticity matrix adopts a diagonal structure, e_{TT} reflecting the self-elasticity coefficient, that quantifies the constraint effect of rising electricity prices on current-period load.

$$E_{rigid} = \begin{bmatrix} e_{11} & 0 & \cdots & 0 \\ 0 & e_{22} & \cdots & 0 \\ \vdots & \vdots & \ddots & \vdots \\ 0 & 0 & \cdots & e_{TT} \end{bmatrix} \quad (23)$$

For flexible loads, capable of time-shifting due to price variations,

$$\begin{aligned} \min W_1 = \frac{1}{H} \times & \left(\sum_{n=1}^N (C_{pur,n}^{grid} - R_{grid,n}^{pv}) - R_{sub}^{es} \times (1+i)^{U-Z} \times \left((1+i)^Z - 1/(1+i)^U - 1 \right) + \left(R_{res} \times i/(1+i)^U - 1 \right) \right. \\ & \left. + \left(\sum_{n=1}^N (C_{con,n}^{pv} + C_{mai,n}^{pv} - R_{sub,n}^{pv}) + C_{con}^{es} + C_{mai}^{es} + C_{rep}^{es} \right) \times \left(i \times (1+i)^U / (1+i)^U - 1 \right) \right) \end{aligned} \quad (30)$$

their elasticity matrix is a full-rank matrix, η_{ik} representing the cross-elasticity coefficient, indicating load transfer tendencies from high-priced to low-priced periods.

$$E_{flex} = \begin{bmatrix} \eta_{11} & \eta_{12} & \cdots & \eta_{1T} \\ \eta_{21} & \eta_{22} & \cdots & \eta_{2T} \\ \vdots & \vdots & \ddots & \vdots \\ \eta_{T1} & \eta_{T2} & \cdots & \eta_{TT} \end{bmatrix} \quad (24)$$

The model satisfies the following economic constraints:

$$\eta_{tt} < 0, \quad \eta_{ik} > 0 (t \neq k), \quad \sum_{k=1}^T \eta_{ik} \leq 0 \quad \forall t \quad (25)$$

(2) Load response calculation method.

Rigid load is solely influenced by the current time period's electricity price, with its mathematical expression defined as:

$$L_{rigid,t} = L_{rigid,t}^0 (1 + e_{tt} \cdot \Delta p_t / p_0) \quad (26)$$

The model degenerates into the traditional fixed load model when $|e_{tt}| \rightarrow 0$.

Flexible load is subject to cross-effects from electricity prices across all time periods, expressed as:

$$L_{flex,t} = L_{flex,t}^0 \left(1 + \sum_{k=1}^T \eta_{tk} \cdot \Delta p_k / p_0 \right) \quad (27)$$

The total load of time period t is the sum of rigid load and flexible load.

(3) Constraints.

1) Energy conservation constraint.

The total electricity consumption of flexible loads remains constant before and after load shifting (assuming no load shedding), expressed as:

$$\sum_{t=1}^T L_{flex,t} = \sum_{t=1}^T L_{flex,t}^0 \quad (28)$$

2) Price constraints

$$p_{\min} \leq p_t \leq p_{\max} \quad (29)$$

4.3. Two-stage optimization configuration model of SES for DPV clusters

4.3.1. First-stage capacity planning model

(1) Objective function.

The primary objective of the first stage is to minimize the leveled annual costs for residential households within the rural distribution network, and the power and capacity of the SES are used as the decision variables, as formulated in Eq. (30).

(2) Constraints.

While a larger SES system enhances the PV self-consumption, it also increases investment costs. Economically, there exists an optimal minimum SES configuration that satisfies the PV self-consumption of village distribution network. The constraints for this stage focus on the local utilization level of DPV within the network, as detailed in Eq. (31).

$$\sum_{t=1}^T \left(\sum_{n=1}^N (E_{sel,n,t} + E_{com,n,t}^{pv}) + E_{cha,t}^{es} \right) \geq \zeta \sum_{t=1}^T \sum_{n=1}^N E_{gen,n,t}^{pv} \quad (31)$$

4.3.2. Second-stage system operation model

(1) Objective function.

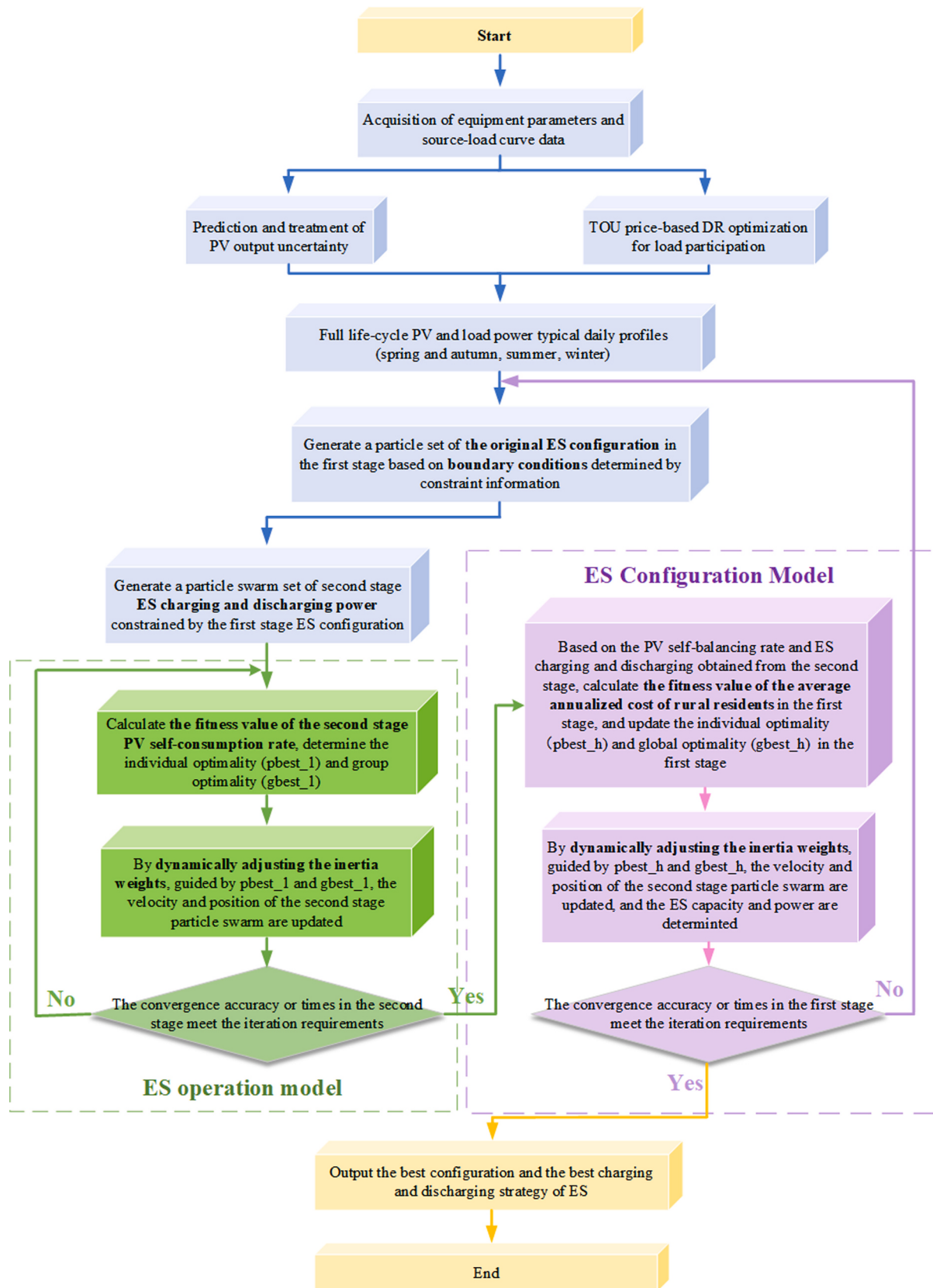


Fig. 3. Flowchart of the APSO for SES configuration.

Table 1

Basic information of the three villages.

Basic information of the three villages	Village 1	Village 2	Village 3
Number of rural households	100	200	300
Investment scale per rural household of DPV (kW)	3	5	4
Coverage rate of DPV (%)	40	100	70
Total investment scale of DPV (kW)	120	1000	840

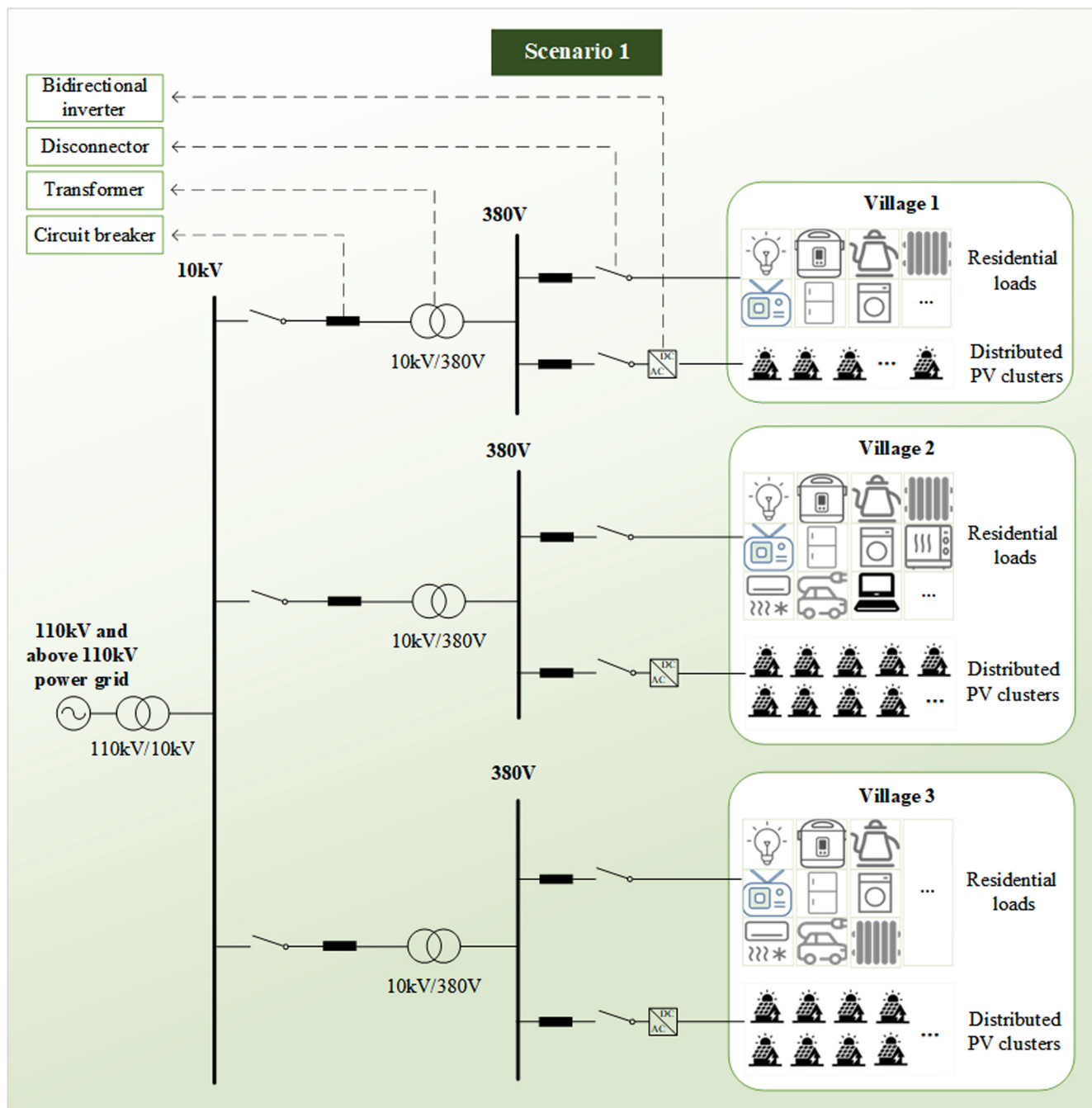
The second stage aims to maximize the PV self-consumption ratio of the distribution network. It optimizes the PV in-situ consumption rate over the project's operational cycle, with the hourly charging and discharging power of the SES system as decision variables, as expressed in Eq. (32).

$$\max W_2 = \left(\sum_{u=1}^U \sum_{n=1}^N \sum_{t=1}^T (E_{sel,n,t}^{pv} + E_{com,n,t}^{pv}) + \sum_{u=1}^U \sum_{t=1}^T E_{cha,t}^{es} \right) / \sum_{u=1}^U \sum_{n=1}^N \sum_{t=1}^T E_{gen,n,t}^{pv} \quad (32)$$

(2) Constraints.

1) Power balance is maintained as Eq. (33).

$$\begin{aligned} \sum_{n=1}^N E_{gen,n,t}^{pv} - \sum_{n=1}^N E_{on,n,t}^{pv} + \sum_{n=1}^N E_{pur,n,t}^{grid} + \sum_{n=1}^N E_{dis,n,t}^{es} \\ = \sum_{n=1}^N E_{sel,n,t}^{pv} + \sum_{n=1}^N E_{com,n,t}^{pv} + \sum_{n=1}^N E_{cha,n,t}^{es} + \sum_{n=1}^N E_{pur,n,t}^{grid} \end{aligned} \quad (33)$$

**Fig. 4.** Topology of the distribution network in Scenario 1.

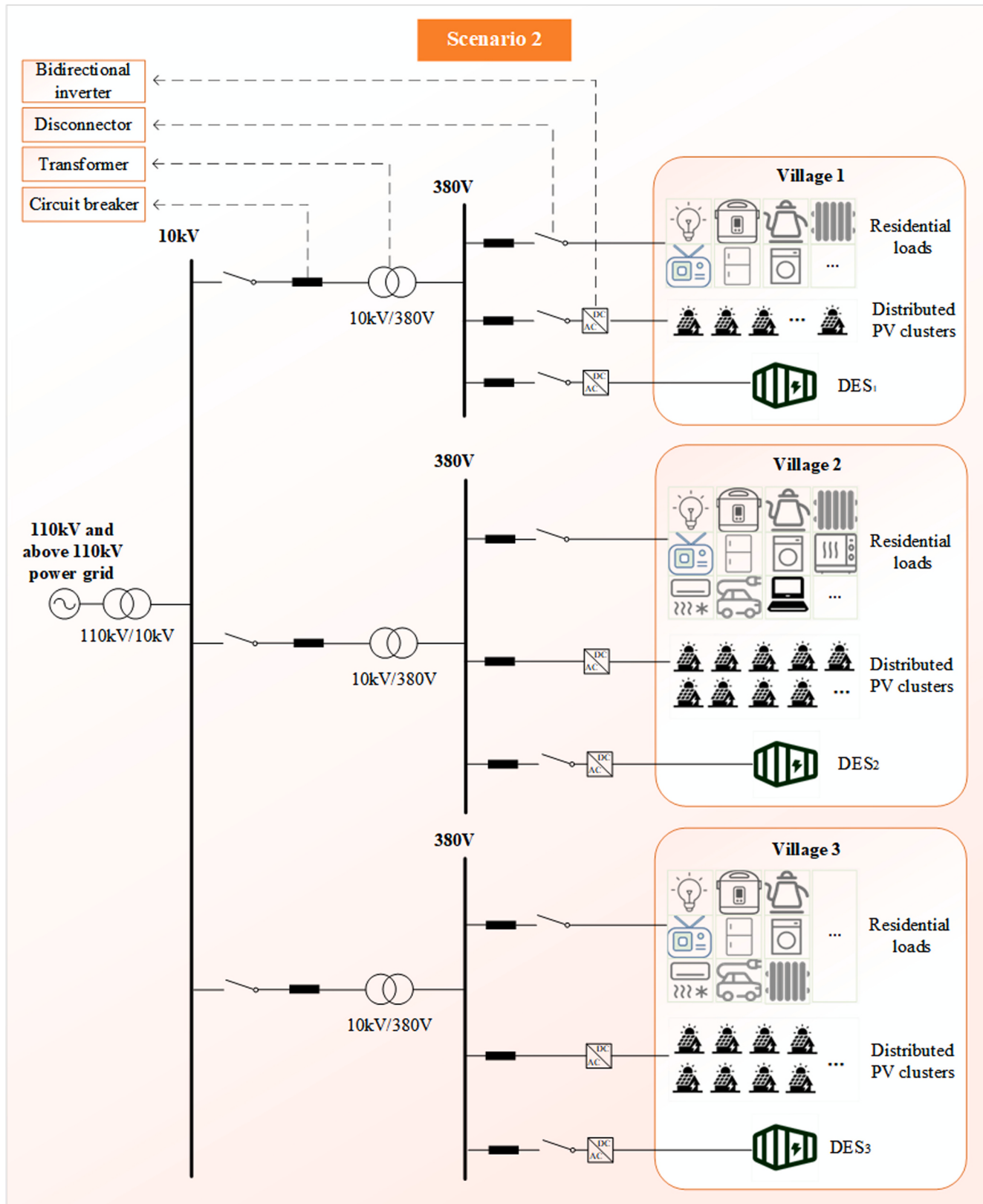


Fig. 5. Topology of the distribution network in Scenario 2.

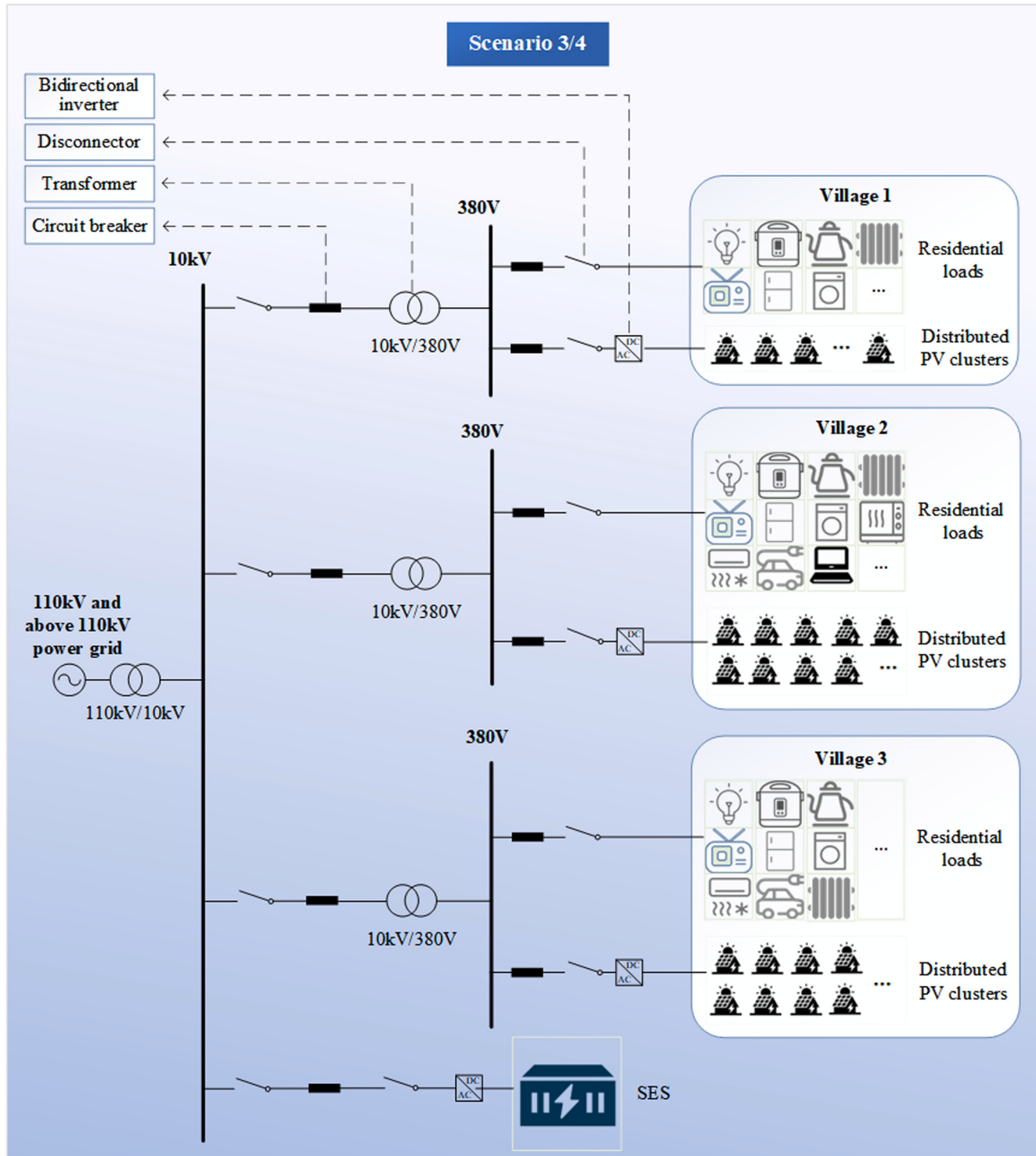


Fig. 6. Topology of the distribution network in Scenarios 3 or 4.

2) The charging and discharging power of the SES battery are constrained by Eqs. (34) to (35).

$$0 \leq \sum_{n=1}^N E_{cha,n,t}^{es} \leq E_{pow}^{es} \quad (34)$$

$$0 \leq E_{dis,n,t}^{es} \leq E_{pow}^{es} \quad (35)$$

3) The battery must avoid simultaneous charging and discharging states, as specified in Eqs. (36) to (38).

$$0 \leq \sum_{n=1}^N E_{cha,n,t}^{es} \leq \alpha_t E_{pow}^{es} \quad (36)$$

$$0 \leq \sum_{n=1}^N E_{dis,n,t}^{es} \leq (1 - \alpha_t) E_{pow}^{es} \quad (37)$$

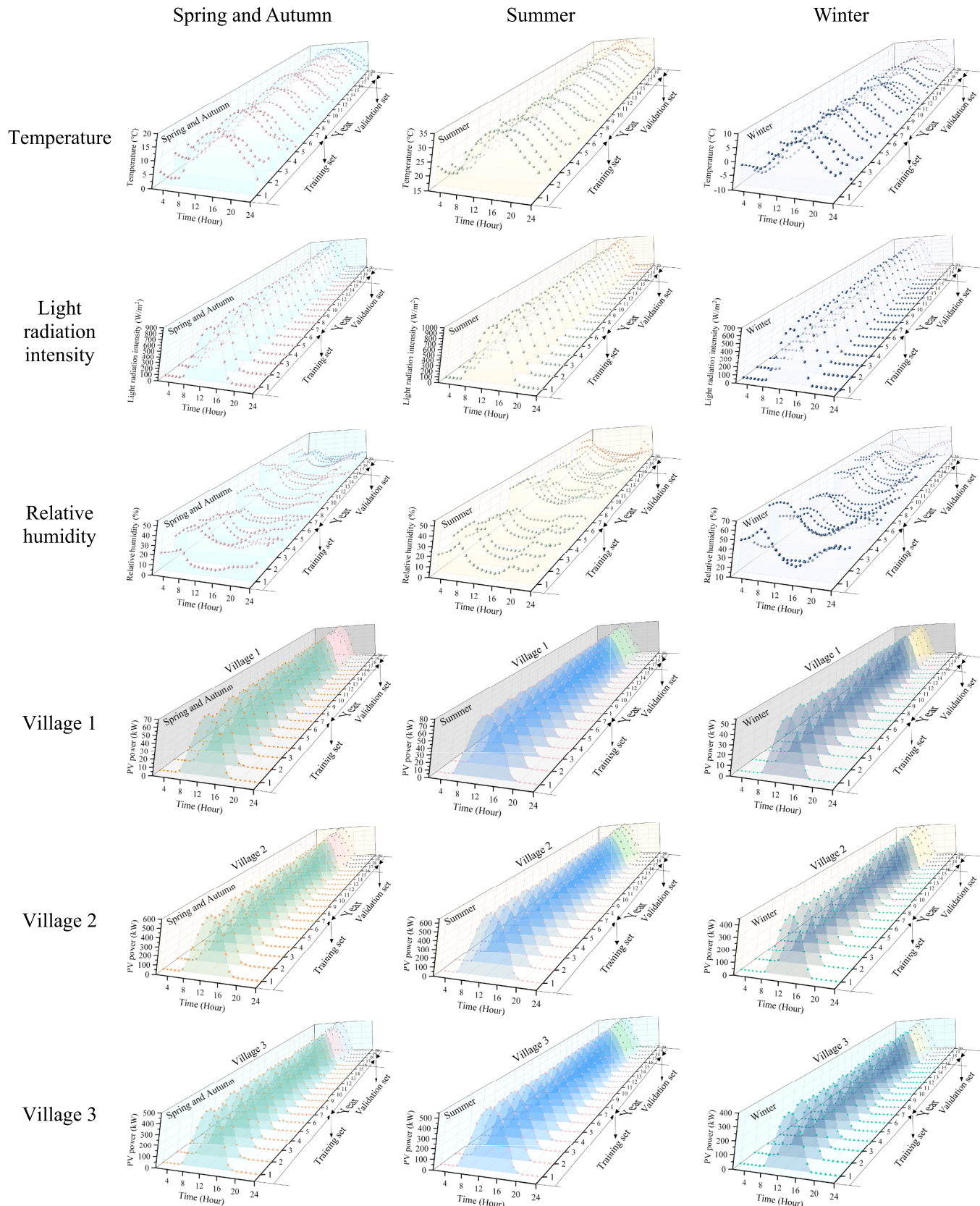


Fig. 7. The training set and validation set for the PV prediction model.

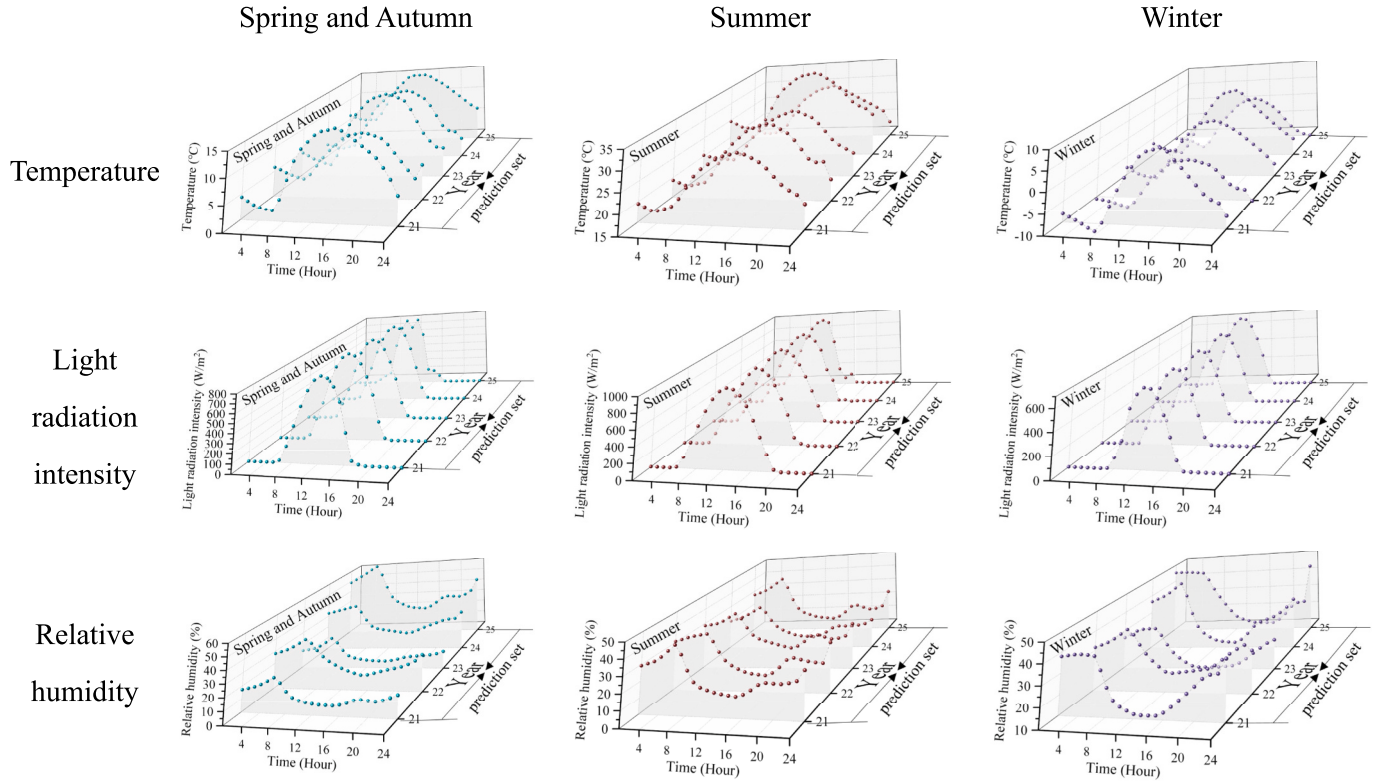


Fig. 8. North China climatic data (Year 21–25): Temp., Radiation & RH.

Table 2

Design parameters of the PV prediction model.

Model parameters	Values
Population size of the genetic algorithm	20
Number of iterations	2000
Mutation probability	0.1
Kernel size of the CNN layer	3
Number of output channels in the CNN layer	16
Hidden size of the GRU layer	4
Number of GRU layers	1
Hidden size of the attention mechanism	4
Learning rate	0.01
Total number of training epochs	5000

$$\alpha_t = \begin{cases} 1 & \sum_{n=1}^N E_{gen,n,t}^{pv} > \sum_{n=1}^N E_{dem,n,t}^{load} \quad \text{and} \quad Q_t^{es} \leq Q_{cap}^{es} \cdot SOC_{max} \\ 0 & \text{else} \end{cases} \quad (38)$$

- 4) The remaining power in the SES at any moment must relate to the previous moment's remaining power, constrained by Eq. (39).

$$Q_t^{es} = Q_{t-1}^{es} + \sum_{n=1}^N E_{cha,n,t}^{es} \times \Delta t \times \varpi_{cha} \quad \text{or} \quad Q_t^{es} = Q_{t-1}^{es} - \sum_{n=1}^N E_{dis,n,t}^{es} \times \Delta t / \varpi_{dis} \quad (39)$$

- 5) To prevent energy loss, the shared storage must adhere to upper and lower limits on the charging state [40], as outlined in Eq. (40).

$$Q_{cap}^{es} \cdot \phi_{min} \leq Q_t^{es} \leq Q_{cap}^{es} \cdot \phi_{max} \quad (40)$$

- 6) Frequent charging and discharging can reduce the battery's lifespan. Therefore, a constraint on the number of charge/discharge cycles is

necessary [41]. For simplicity, Eq. (41) approximates one charge/discharge cycle per day, excluding capacity decay considerations.

$$\sum_{t=1}^{24} \sum_{n=1}^N E_{dis,n,t}^{es} / \varpi_{dis} \leq Q_{cap}^{es} \cdot \phi_{max} \quad (41)$$

4.4. Model solution method

The optimal configuration of ES capacity involves multiple constraints that are difficult to solve using traditional mathematical methods. The Particle Swarm Optimization (PSO) algorithm obtains optimal solutions by simulating interactions and evolution among individuals in a population, making it suitable for multidimensional optimization problems. However, it also has limitations, such as susceptibility to local optima and sensitivity to parameter selection. Empirical studies show that a larger inertia weight enhances global convergence, while a smaller one improves local convergence. Thus, the choice of inertia weight critically affects PSO performance. To balance global and local search, the inertia weight can be set as a function of iteration count, enabling stronger global exploration in early stages for faster search and enhanced local exploitation in later stages for higher convergence precision.

An improved adaptive inertia weight particle swarm optimization algorithm (APSO) is employed to solve the two-stage optimal allocation model for village-domain DPV cluster and SES [42]. The inertia weights are updated using the specified eq. (42).

$$w_g^d = \begin{cases} w_{min} + (w_{max} - w_{min}) \times \left(f(x_g^d) - f_{min}^d / f_{average}^d - f_{min}^d \right) & f(x_g^d) \leq f_{average}^d \\ w_{max} & f(x_g^d) > f_{average}^d \end{cases} \quad (42)$$

The average fitness of all particles at the d^{th} iteration is expressed by the eq. (43):

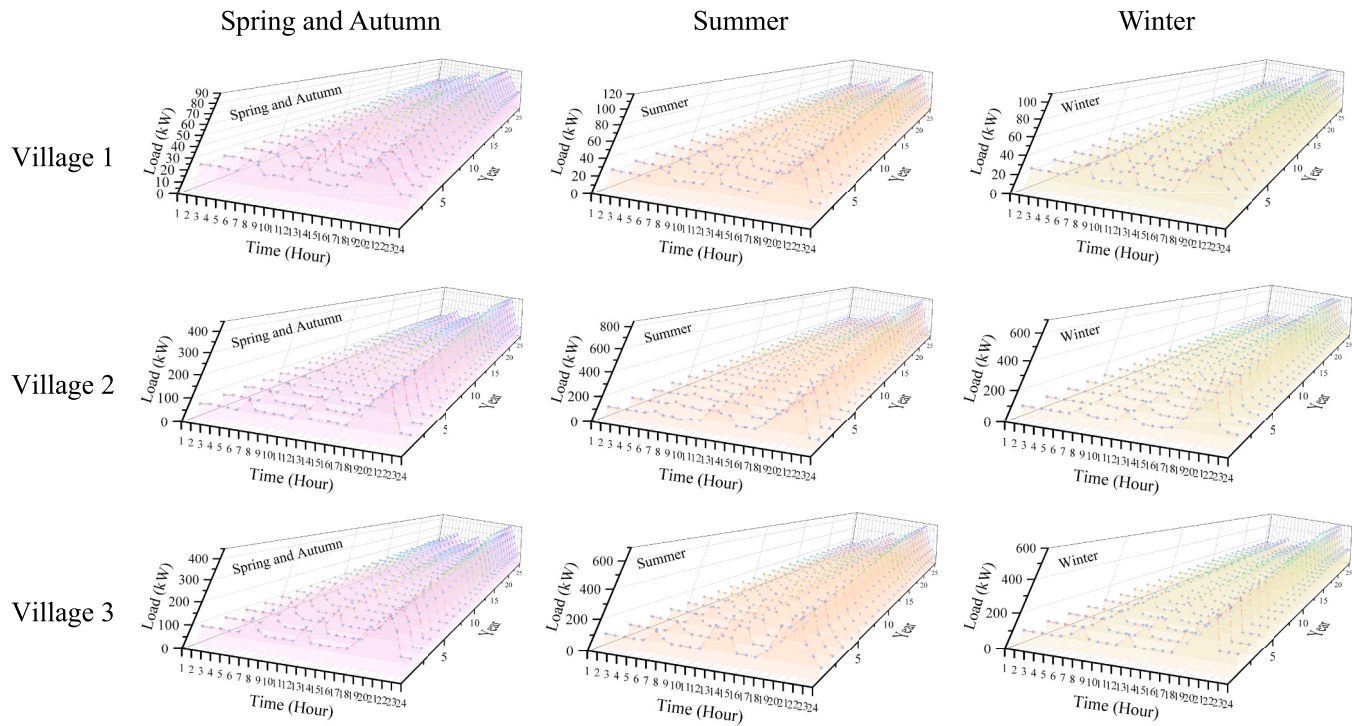


Fig. 9. Load power of typical households on typical days in different villages.

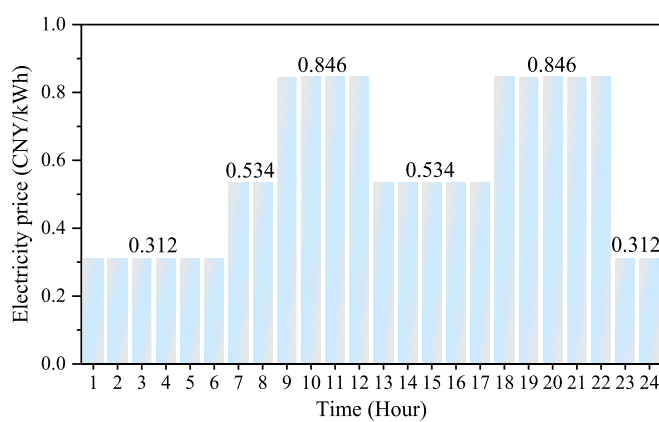


Fig. 10. The peak and valley levels of the power grid with corresponding tariffs.

$$f_{average}^d = \sum_{g=1}^G f(x_g^d) / G \quad (43)$$

The minimum fitness among all particles at the d^{th} iteration is defined by the eq. (44):

$$f_{min}^d = \min \{ f(x_1^d), f(x_2^d), \dots, f(x_g^d) \} \quad (44)$$

The schematic representation of the algorithm is illustrated in Fig. 3.

Table 3

The average proportions of flexible load in the three villages during peak, flat, and valley periods.

Season	Village 1			Village 2			Village 3		
	Peak	Flat	Valley	Peak	Flat	Valley	Peak	Flat	Valley
Spring and Autumn	10.90 %	0.00 %	0.00 %	19.17 %	6.30 %	0.00 %	14.04 %	2.76 %	0.00 %
Summer	22.15 %	3.89 %	0.00 %	29.29 %	10.52 %	0.00 %	25.39 %	6.45 %	0.00 %
Winter	21.51 %	2.31 %	0.00 %	25.01 %	10.87 %	0.00 %	24.06 %	6.28 %	0.00 %

5. Case study

5.1. Construction of typical scenarios and design of basic data

5.1.1. Construction of typical scenarios

To analyze the impacts of residual power complementarity, SES configuration, and DR implementation on the PV self-consumption and power self-sufficiency, and the leveled annual cost per rural household, four distinct scenarios are designed as follows:

- **Scenario 1:** No ES configuration. DPV systems in each village operate independently without ES, and no DR is implemented.
- **Scenario 2:** DES configuration. DPV clusters within the rural distribution network adopt a self-generation and self-consumption model with surplus power connected into the grid. Each village independently invests in ES, and no DR is implemented.
- **Scenario 3:** Residual power complementarity and SES configuration. DPV clusters within the rural distribution network operate under a self-generation and self-consumption model with residual power complementarity. All villages jointly invest in a SES system, and no DR is implemented.
- **Scenario 4:** Residual power complementarity, SES configuration, and DR implementation. DPV clusters within the rural distribution network operate under a self-generation and self-consumption model with residual power complementarity. All villages jointly invest in a SES system, and DR is implemented.

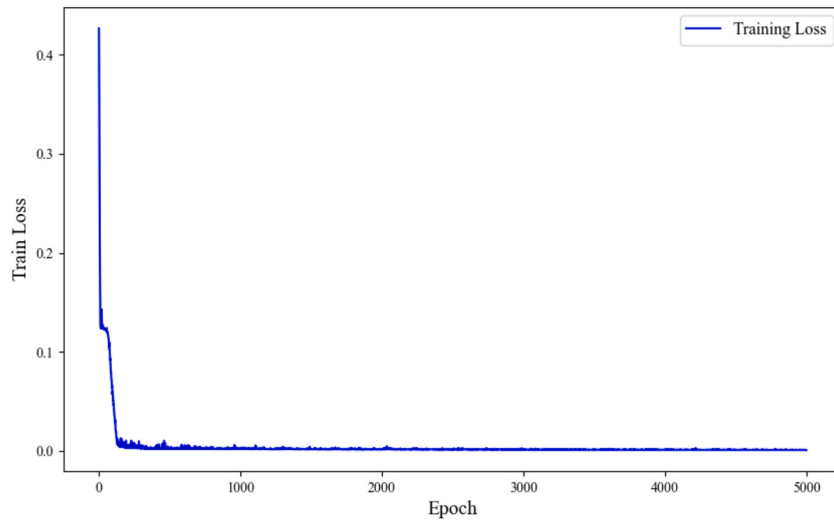
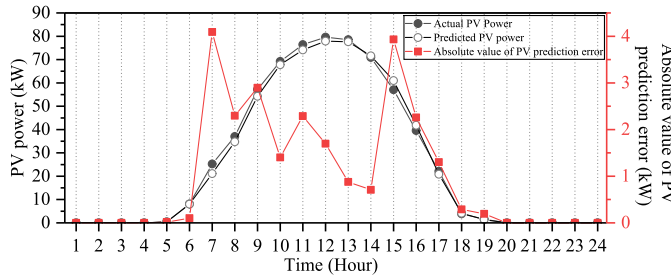
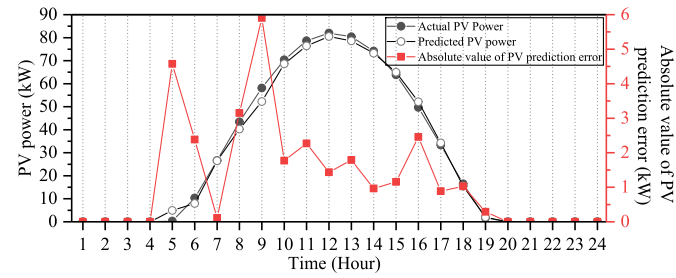


Fig. 11. The variation of the loss function during training.

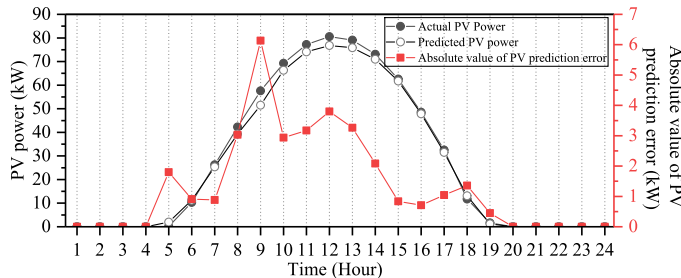
The 17th year of the planning period



The 18th year of the planning period



The 19th year of the planning period



The 20th year of the planning period

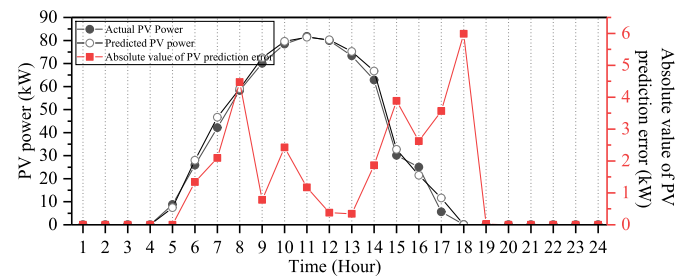


Fig. 12. Temporal variations of actual output, predicted output, and prediction errors in the validation set for village 1 during summer period.

5.1.2. Design of basic data

(1) The status of rural distribution networks.

This paper focuses on a DPV promotion area within a rural distribution network in North China. The village distribution network covers three neighboring villages, all within the power supply range of the same township-level grid, with a linear distance of less than 5 km. This aligns with China's typical rural power supply structure of "transformer district-village group." The study's grouping method follows the standard rural distribution network framework, with the natural village as the smallest unit. The grid encompasses three villages, each differing in population size, economic status, and DPV investment levels:

- **Village 1:** Economically disadvantaged village with only basic electrical equipment, resulting in low overall electricity consumption.
- **Village 2:** Affluent village with a diverse range of electrical equipment, often operating simultaneously, leading to high overall electricity consumption.
- **Village 3:** Generally affluent village with high-power electrical devices, but shorter operating durations for equipment, resulting in moderate overall electricity consumption.

The number of rural households, residential power consumption, and DPV investment for the three villages are summarized in the Table 1:

This paper adopts a radial topology for the rural distribution network, where three villages are connected to a shared transformer via a 10 kV trunk line, with each village receiving 380 V low-voltage supply. The network topologies for Scenarios 1 to 4 are illustrated Fig. 4–6.

Table 4
Deviation between actual and predicted PV output in summer for Village 1.

Time	PV power prediction deviation (kW)			
	Year 17	Year 18	Year 19	Year 20
1:00/2:00/3:00/4:00	0.00	0.00	0.00	0.00
5:00	0.01	4.58	1.80	0.00
6:00	0.10	2.38	0.91	1.34
7:00	4.09	0.11	0.88	2.10
8:00	2.30	3.15	3.03	4.47
9:00	2.89	5.90	6.13	0.78
10:00	1.40	1.77	2.94	2.43
11:00	2.29	2.27	3.17	1.17
12:00	1.70	1.43	3.80	0.38
13:00	0.88	1.79	3.26	0.34
14:00	0.71	0.97	2.08	1.86
15:00	3.93	1.16	0.84	3.88
16:00	2.26	2.46	0.71	2.62
17:00	1.30	0.89	1.04	3.56
18:00	0.29	1.03	1.36	5.99
19:00	0.19	0.29	0.45	0.02
20:00/21:00/22:00/23:00/24:00	0.00	0.00	0.00	0.00
Average actual PV power (kW)		28.30		
Average PV prediction deviation (kW)		1.28		
PV prediction accuracy (%)		95.52		

(Scenarios 3 and 4 share the same topology).

(2) DPV clusters output.

Considering the influence of three key factors, namely temperature, solar radiation and relative humidity, on PV output in North China, the GA-CNN-GRU attention-based prediction model introduced in Section 4.1 is applied for multi-scale forecasting. Historical data covering PV output, temperature, solar radiation and relative humidity from Villages 1 to 3 during the first 20 years of the planning period are utilized. Data from years 1 to 16 are used as the training set, while data from years 17 to 20 serve as the validation set. The training set and validation set for the PV prediction model are shown in Fig. 7.

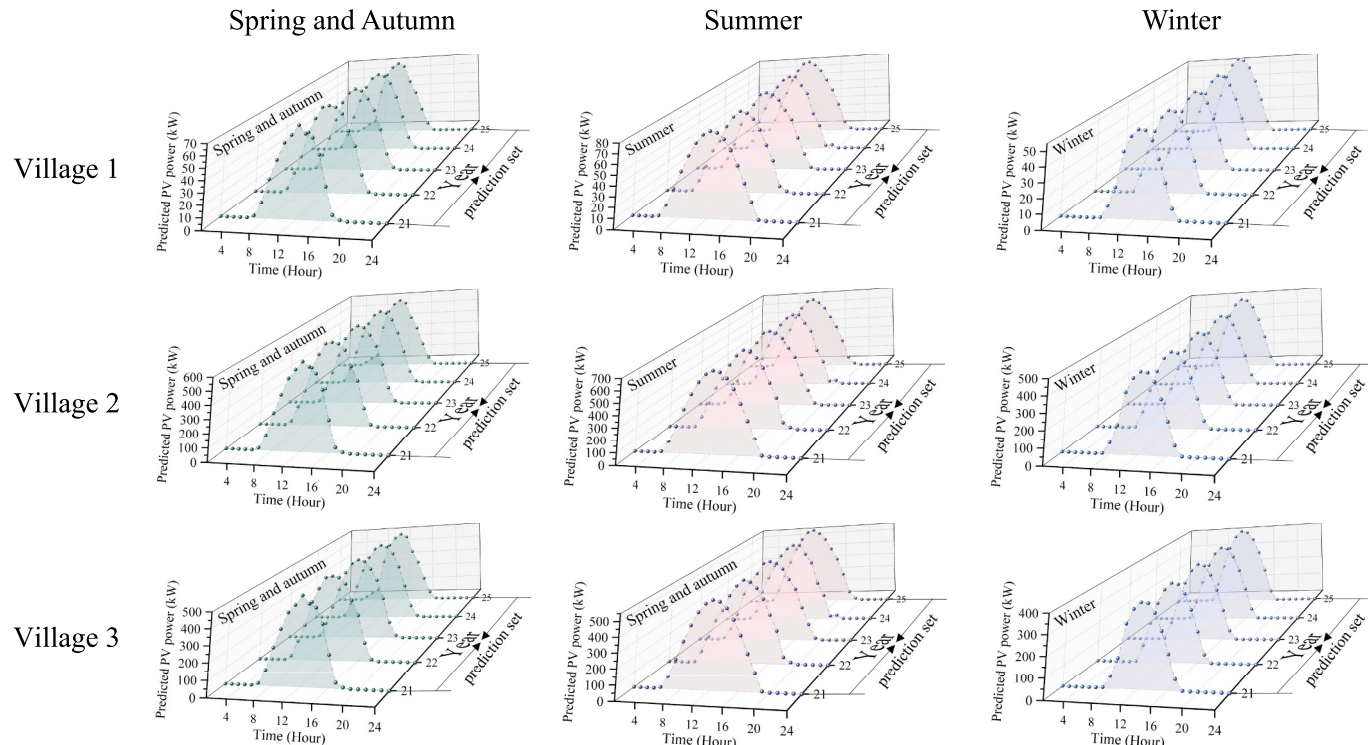


Fig. 13. PV output forecasting for Years 21–25 of the planning period across Villages 1–3.

Once the model achieves satisfactory performance, training is terminated, and the optimized model is used to forecast PV output for years 20–25. The corresponding environmental data (temperature, solar radiation, and relative humidity) for North China during this period are shown in Fig. 8.

The PV prediction model parameters are configured as shown in the Table 2:

(3) Rural loads.

Based on statistical yearbook data (2010–2024) from a rural area in North China [43], the average annual growth rate of residential electricity load is 3.06 %. Following the 20-year planning standard in Guide for choice power transformers (GB/T 17468–2019) and accounting for rural electrification trends [44], a segmented load growth model is adopted: the first 20 years maintain a 3.06 % annual increase, followed by a 5-year saturation period (0 % growth). Fig. 9 illustrates the load power variations across typical days of different seasons for three villages during the planning period.

(4) Residential electricity pricing.

The TOU periods and corresponding tariffs for the power grid are shown in the figure below. The flat-rate price is adopted as the benchmark electricity price. The self-elasticity of rigid load is denoted as $e_{tt} = -0.02$, and the elasticity matrix of flexible load is given by $E_{flex} = \begin{bmatrix} -0.4 & 0.2 & 0.1 \\ 0.1 & -0.3 & 0.1 \\ 0.05 & 0.1 & -0.2 \end{bmatrix}$.

The peak and valley levels of the power grid with corresponding tariffs are depicted in Fig. 10.

The average proportions of flexible load in the three villages during peak, flat, and valley periods are presented in the Table 3.

(5) Equipment economics and technical parameters.

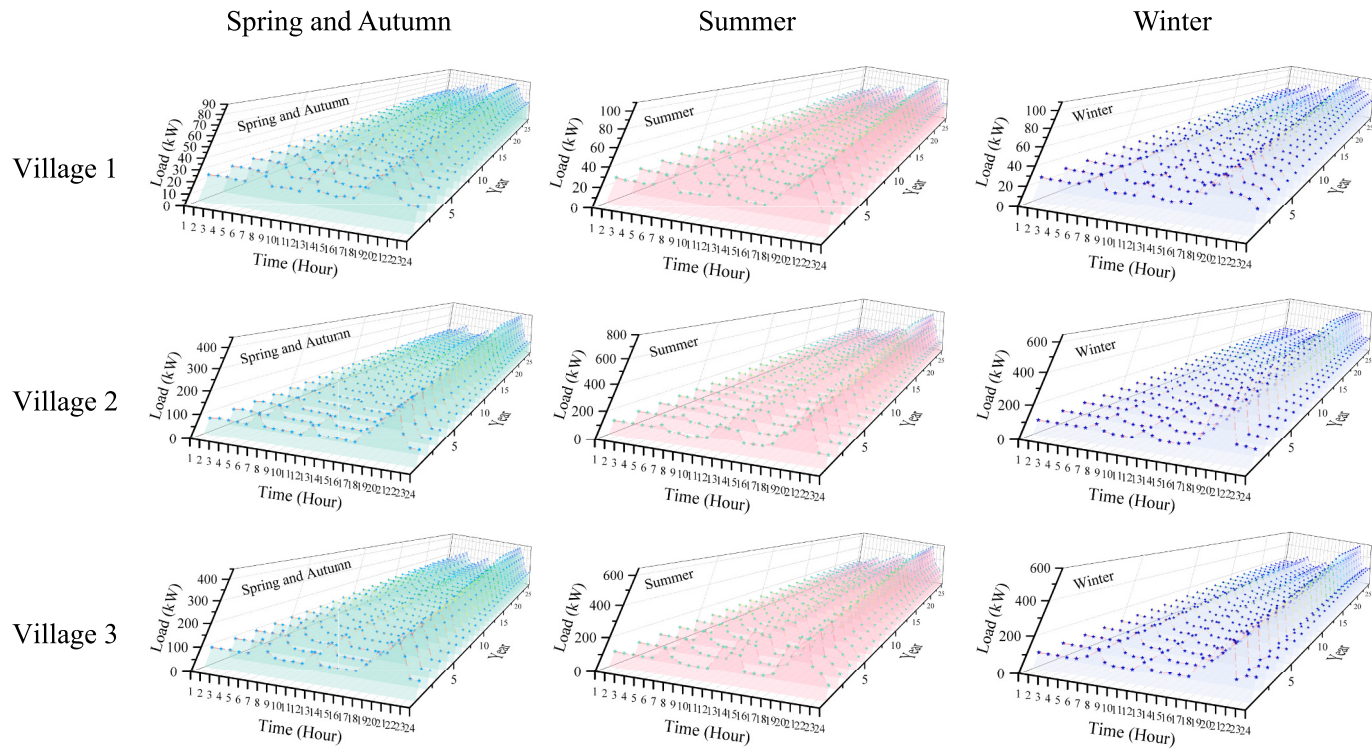


Fig. 14. Seasonal typical daily load curves of rural households after TOU price-based DR implementation.

Table 5

The calculation results of the evaluation indicators for the implementation effect of TOU price-based DR.

Village	Evaluation indicators	Before implementing TOU price-based DR			After implementing TOU price-based DR		
		Spring and autumn	Summer	Winter	Spring and autumn	Summer	Winter
Village 1	Average maximum Load (kW)	71.71	91.22	91.85	68.53	85.01	86.20
	Average minimum Load (kW)	30.60	30.60	31.00	37.96	30.82	31.00
	Average peak-valley load difference (kW)	41.11	60.62	60.85	30.57	54.19	55.19
	Average peak-valley difference ratio (%)	57.33	66.46	66.24	44.61	63.74	64.03
Village 2	Average maximum Load (kW)	377.37	649.90	536.41	358.79	609.71	503.36
	Average minimum Load (kW)	83.38	106.15	105.69	85.64	104.65	107.09
	Average peak-valley load difference (kW)	293.99	543.75	430.72	273.15	505.06	396.26
	Average peak-valley difference ratio (%)	77.9	83.67	80.30	76.13	82.84	78.72
Village 3	Average maximum Load (kW)	368.83	551.50	501.47	353.24	516.49	473.09
	Average minimum Load (kW)	109.31	110.53	110.22	110.82	116.35	114.31
	Average peak-valley load difference (kW)	259.52	440.97	391.25	242.42	400.14	358.77
	Average peak-valley difference ratio (%)	70.36	79.96	78.02	68.63	77.47	75.84
All villages	Average maximum Load (kW)	447.30	654.82	595.21	435.98	640.74	580.41
	Average minimum Load (kW)	189.00	213.85	204.28	201.03	240.60	223.64
	Average peak-valley load difference (kW)	258.30	440.97	390.94	234.95	400.14	356.77
	Average peak-valley difference ratio (%)	57.75	67.34	65.68	53.89	62.45	61.46

The economic parameters for DPV systems include: a unit capacity investment of 3.04 CNY/W, installation cost of 0.45 CNY/W, and feed-in tariff of 0.292 CNY/kWh. The PV system has a 25-year service life with annual operation and maintenance costs equivalent to 1 % of the initial investment. The residual value of fixed assets is calculated at 5 % of the initial investment, with an initial installation subsidy of 0.2 CNY/W.

For SES systems, the lifecycle is 10 years with unit capacity costs of 800 CNY/kWh and unit power costs of 300 CNY/kW. The installation costs are incorporated into the initial investment, with annual operation and maintenance expenses at 3 % of the initial investment. The system operates within a state of charge range of 0.20–0.95, with 90 % charging/discharging efficiency [45]. A government subsidy of 0.3 CNY/kWh is provided based on actual discharge amounts for five consecutive years, with an asset discount rate of 7 %.

In villages with sufficient DPV generation, electricity is transmitted via low-voltage distribution networks to areas with PV deficits, or from

distributed PV systems to SES (charging), and from shared storage to villages. This transmission incurs line losses. According to the State Grid Corporation Line Loss Management Standards, the line loss rate for grids below 110 kV should not exceed 7 %. In this study, the grid line loss rate is set at 5 %.

5.2. Results analysis of PV prediction and DR

5.2.1. The results of PV prediction

A GA-CNN-GRU PV prediction model incorporating an attention mechanism is employed to perform multi-time-scale forecasting based on historical data and model parameters from the first 20 years of the planning period, as specified in Section 5.1.2. Specifically, data from years 1–16 serve as the training set, while data from years 17–20 are used for validation. The model was trained for 5000 epochs using the AdamW optimizer in Python. The variation of the loss function during

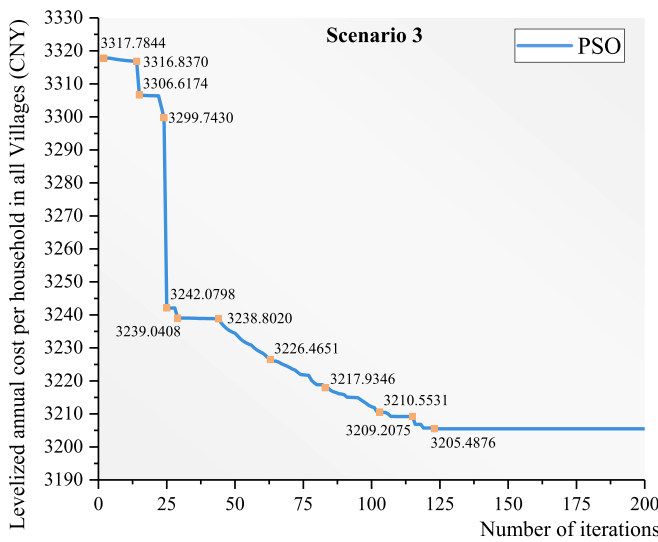


Fig. 15. Fitness curve of the PSO algorithm.

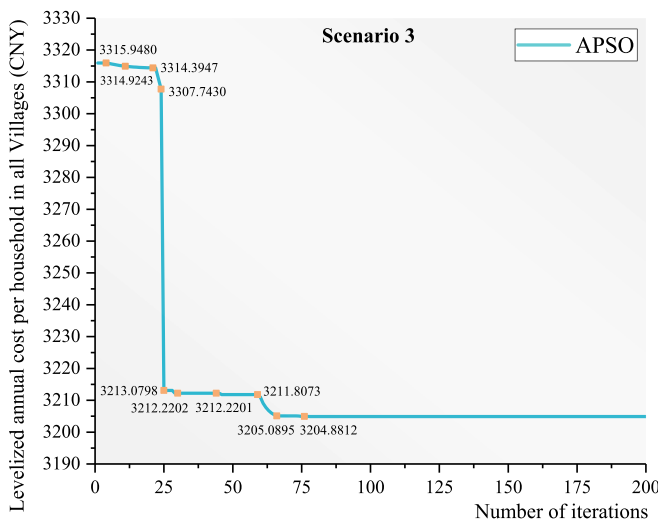


Fig. 16. Fitness curve of the APSO algorithm.

training is illustrated in Fig. 11.

The loss function quantifies the mean squared error between the model's predicted output and actual measurements. Its convergence behavior reflects the model's training dynamics and learning efficiency. As shown in Fig. 11, the loss converges to approximately 0.00 after 2000 training epochs and remains stable, indicating strong fitting capability

and accurate capture of the nonlinear characteristics of PV output.

Using summer data from Village 1 as an example, prediction deviation and model accuracy are assessed by comparing predicted values with actual data from years 17–20, as illustrated in Fig. 12.

The specific numerical values of PV prediction errors in the validation set for Village 1 during summer are presented in the Table 4.

As evidenced by the results in Table 4, the proposed GA-CNN-GRU model with enhanced attention mechanism demonstrates superior forecasting performance. Taking the summer PV output prediction of Village 1 as an example, the model achieves 95.52 % prediction accuracy on the validation set, confirming its exceptional capability in capturing critical meteorological features. Building upon this validation, the model application is extended to PV output forecasting for Years 21–25 of the planning period. Fig. 13 presents the prediction results across Villages 1–3.

This paper utilizes the time-series PV output data from three village clusters during the 25-year planning period as key input parameters for the ES optimization configuration model, establishing the data foundation for subsequent ES system optimization research in Sections 5.3 and 5.4.

5.2.2. The results of TOU price-based DR implementation

The seasonal typical daily load curves of rural households after TOU price-based DR implementation are shown in Fig. 14:

The calculation results of the evaluation indicators for the implementation effect of TOU price-based DR are shown in the Table 5.

Table 5 demonstrates that the TOU-based DR mechanism significantly optimizes rural load profiles. Taking the aggregated load of all

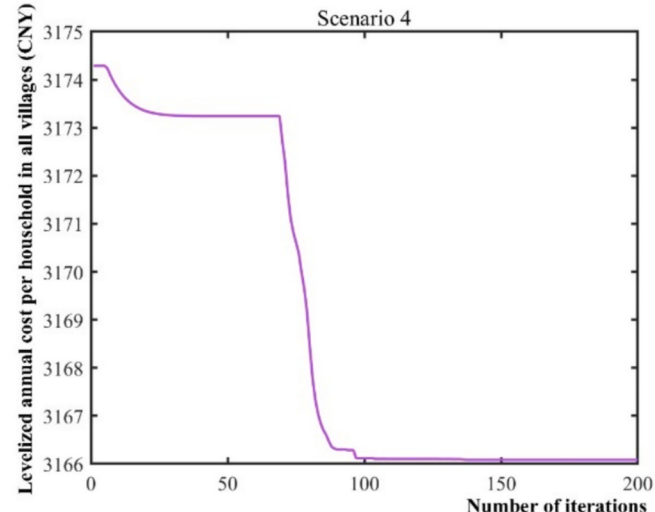


Fig. 18. Adaptability curve in Scenario 4.

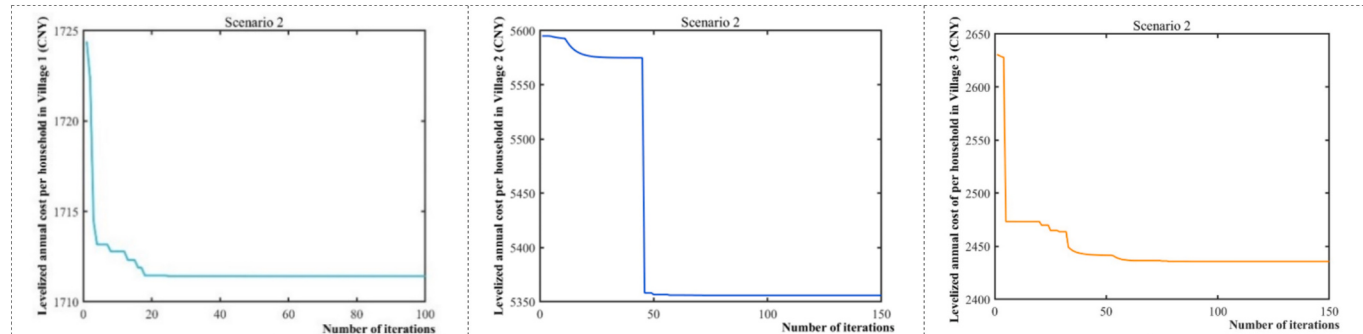


Fig. 17. Adaptability curve in Scenario 2.

Table 6

ES configuration results in different scenarios.

Optimization results	Scenario 2				Scenario 3	Scenario 4
	Village 1	Village 2	Village 3	All villages	All villages	All villages
ES capacity (kWh)	140	4189	2015	6344	6147	5855
ES power (kW)	24	751	392	1167	1045	1027
Initial investment of ES (CNY)			5,425,177		5,231,749	4,991,814
The ES investment costs saved in Scenario 3 and 4 (CNY)			/		193,428	433,363
The savings proportion of ES investment costs in scenarios 3 and 4 (%)			/		3.57	7.99

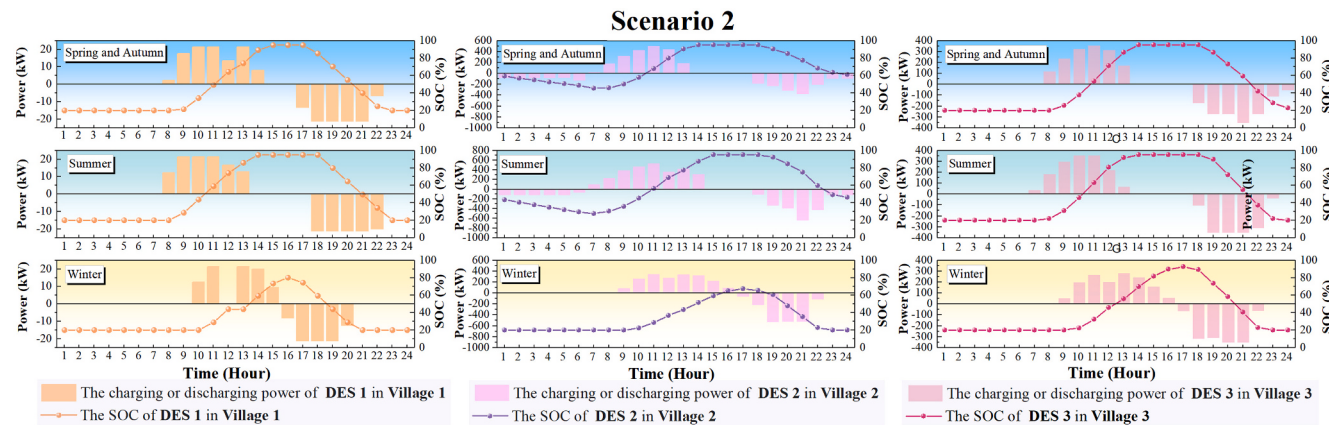


Fig. 19. Operation performance of DES systems in Scenario 2.

villages in the distribution network as an example, during spring/autumn, summer, and winter typical days, the peak average load decreased by 2.53 %, 2.15 %, and 2.49 %, respectively, while the valley average load increased by 6.37 %, 12.51 %, and 9.48 %. Consequently, the peak-valley difference rate dropped by 3.86 %, 4.89 %, and 4.22 %. This optimization mitigates grid peak-shaving pressures. Notably, rural users actively shifted consumption from high-price peak periods to low-price valleys in response to pricing signals, reducing grid operational costs and lowering electricity expenses, thereby achieving a win-win outcome for both grid operators and rural households.

5.3. Optimization process of ES configuration under different scenarios

5.3.1. Comparison of solution methods

This study employs standard PSO and an APSO to solve the ES optimization problem. Multiple experiments were conducted with varying initial populations and iteration counts to observe algorithmic convergence under different parameter settings. Using Scenario 3 as a benchmark case, Fig. 15 and Fig. 16 compare the convergence performance of both methods under identical computational conditions. The modified PSO demonstrates superior convergence stability and speed compared to the standard PSO. Results indicate that the adaptive inertia weight adjustment enables more efficient escape from local optima and accelerates global optimization. Thus, the APSO algorithm proves more effective for solving the ES configuration model proposed in Section 4.3.

5.3.2. ES configuration optimization across scenarios

An improved particle swarm optimization (PSO) algorithm with adaptive inertia weight was implemented to optimize ES configurations across different scenarios. The algorithm parameters were configured as follows: swarm size of 100 particles with cognitive and social factors both set to 0.5, initial inertia weight of 0.8, and iteration limits of 100 or 150 for Scenario 2 and 200 for Scenarios 3–4. As detailed in Section 5.2.1, the optimization process for Scenario 3 demonstrated convergence characteristics, while the corresponding fitness convergence

curves for Scenarios 2 and 4 are presented in Fig. 17 and 18, respectively.

5.4. Comparative analysis of ES configuration and system operation results under different scenarios

5.4.1. ES configuration results

Table 6 presents the ES configurations for three villages under different scenarios.

In scenario 2, each village is equipped with a DES system, resulting in a total capacity of 6344 kWh and power of 1167 kW. The initial investment reaches 5,425,177 CNY, with a leveled annual cost of 3288 CNY per rural household.

In Scenario 3, three villages are equipped with a SES system with a capacity of 6147 kWh and a power of 1045 kW, reducing the initial investment to 5,231,479 CNY and leveled annual cost to 3205 CNY. This configuration demonstrates a 3.57 % reduction in initial investment and 2.54 % decrease in leveled annual cost compared to Scenario 2.

Scenario 4, incorporating TOU price-based DR, further optimizes the SES configuration to 5855 kWh capacity and 1027 kW power. The initial investment decreases to 4,991,814 CNY (a 7.99 % reduction from Scenario 2), and the leveled annual cost decreases to 3166 CNY (3.72 % lower than Scenario 2). The implementation of shared SES for multi-DPV clusters in rural distribution networks demonstrates superior cost-effectiveness compared to DES configurations. Furthermore, the economic viability of the shared storage solution is significantly enhanced through the integration of TOU price-based DR mechanisms.

5.4.2. Comparative analysis of ES operation

In long-term operation of DPV systems, interannual variations in PV output and load power are predominantly seasonal. Within the same climatic region, meteorological differences across years mainly cause short-term fluctuations, while maintaining highly stable long-term statistical characteristics. Accordingly, this study analyzes typical seasonal-day data (Mid-period: the 12-th year) representing near-average PV

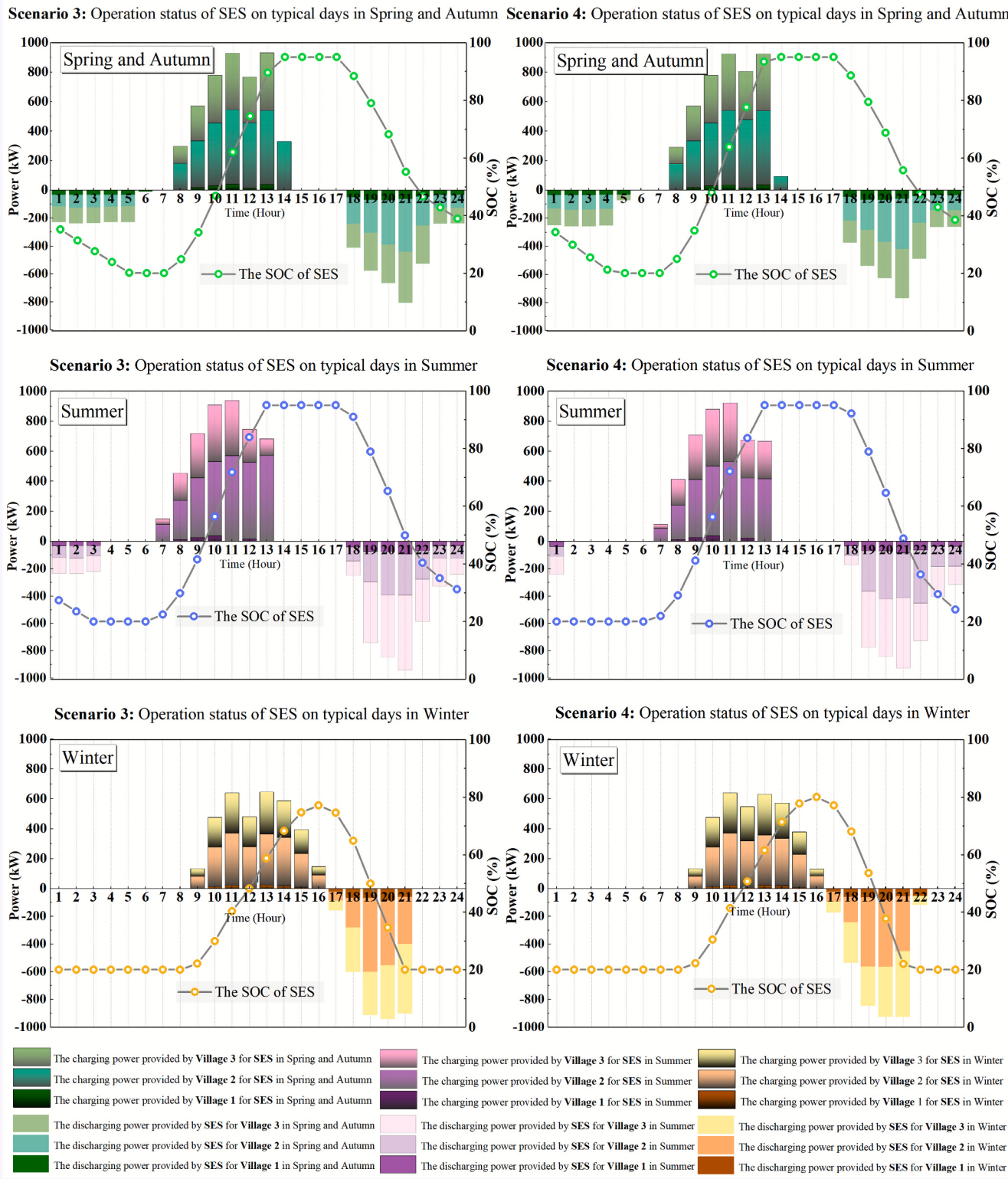


Fig. 20. Operation performance of SES in Scenario 3 and 4.

output and load power conditions.

Fig. 19 illustrates the SOC variation and charge-discharge power trends of DES systems in three villages.

In Scenario 2, the limitations of DES become evident. For example, during spring and autumn, Village 1 begins discharging at 17:00 due to insufficient PV output, earlier than other villages, while Village 2 discharges continuously from 18:00 until 6:00 the next day. This lack of

coordination in charging and discharging timing leads to significant disparities in PV utilization. Additionally, compared to SES (Scenarios 3 and 4), DES exhibits more concentrated charge discharge periods, resulting in lower system capacity utilization. The SOC also shows higher instability and greater fluctuations.

Fig. 20 presents the operational performance of SES in Scenarios 3 and 4.

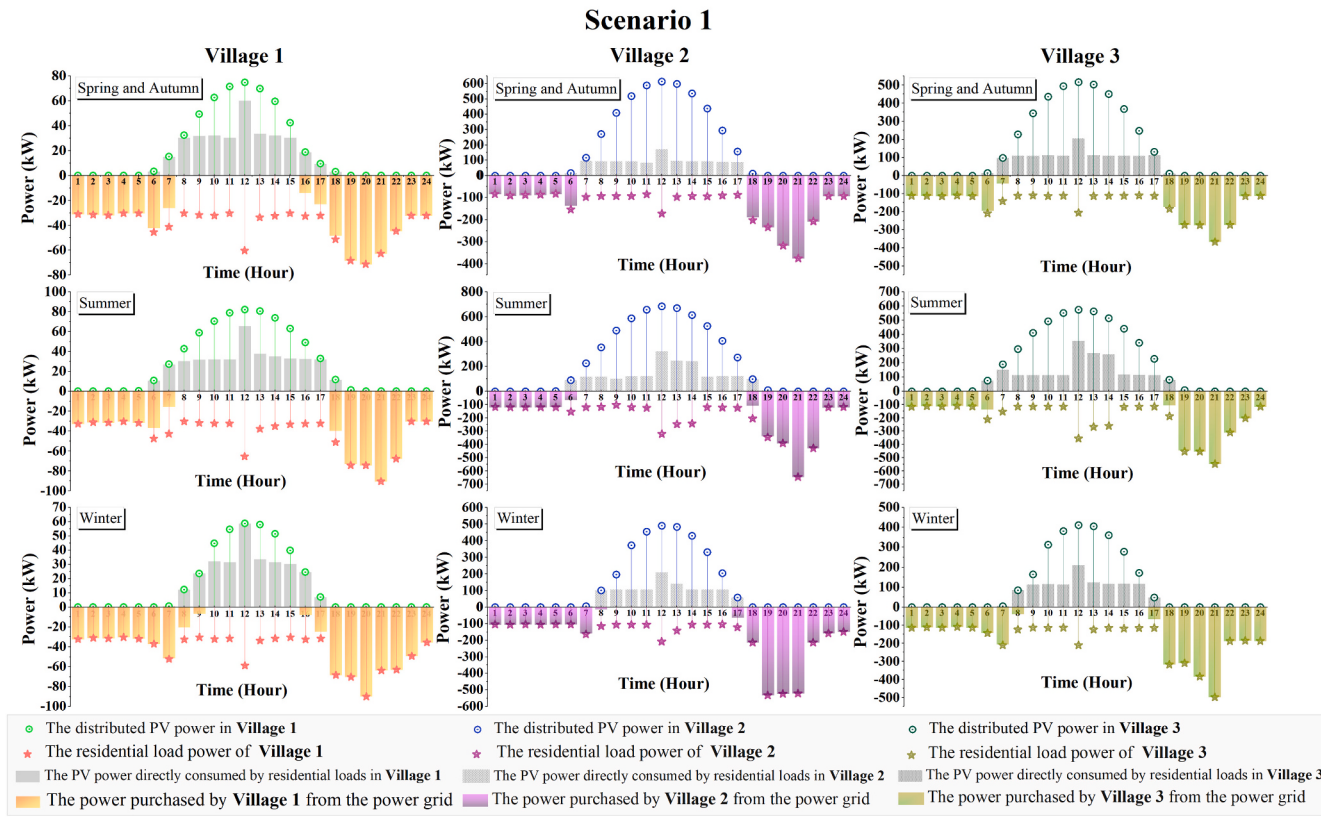


Fig. 21. The situation of PV-self consumption and self-sufficiency in different villages in Scenario 1.

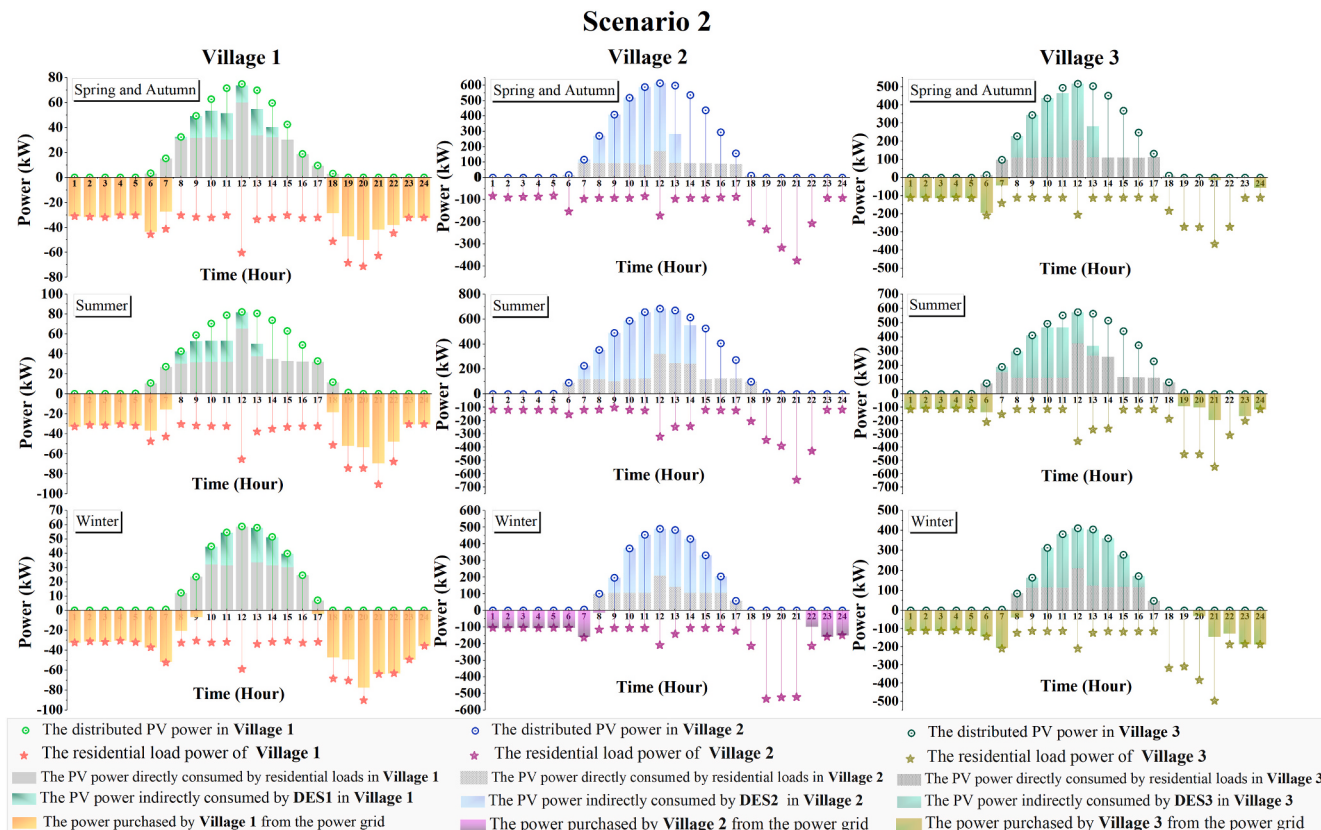


Fig. 22. The situation of PV-self consumption and self-sufficiency in different villages in Scenario 2.

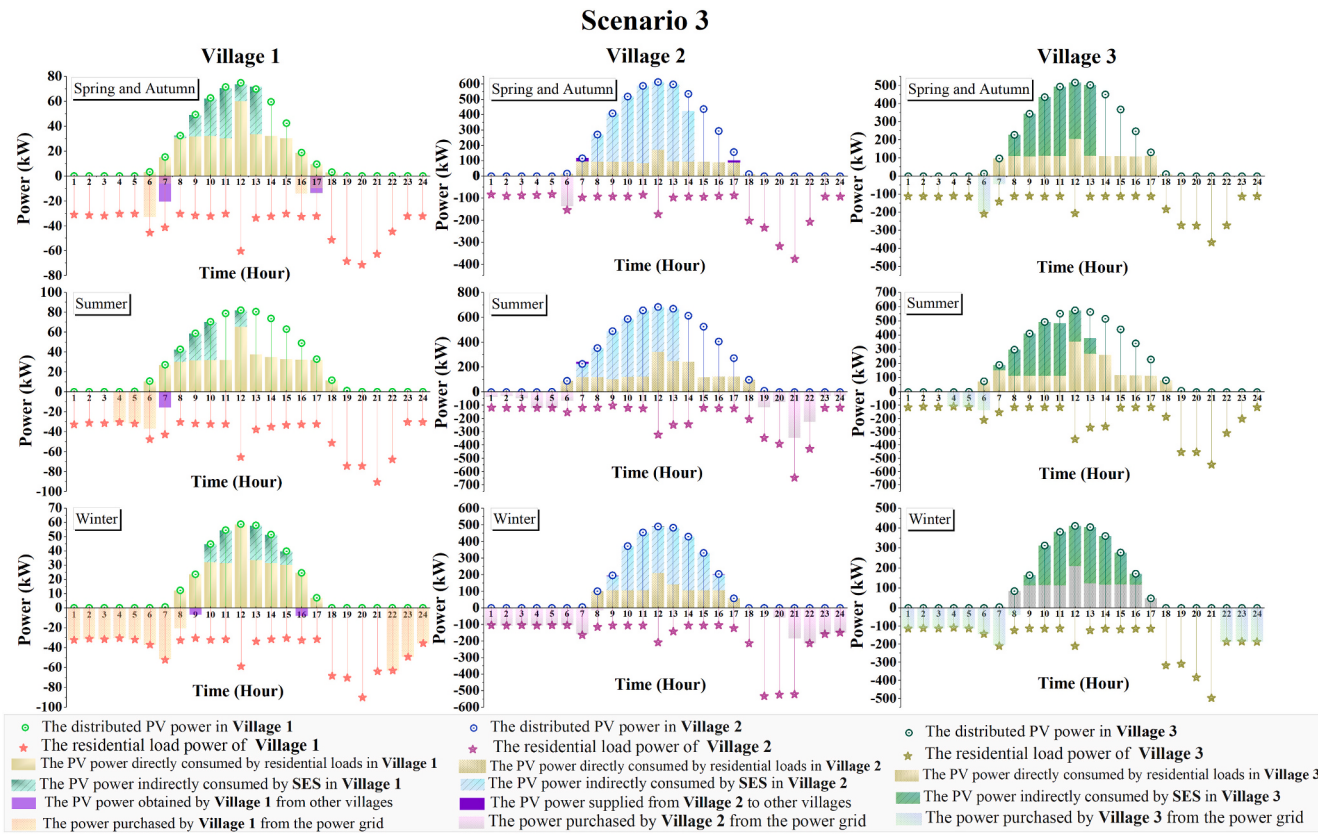


Fig. 23. The situation of PV-self consumption and self-sufficiency in different villages in Scenario 3.

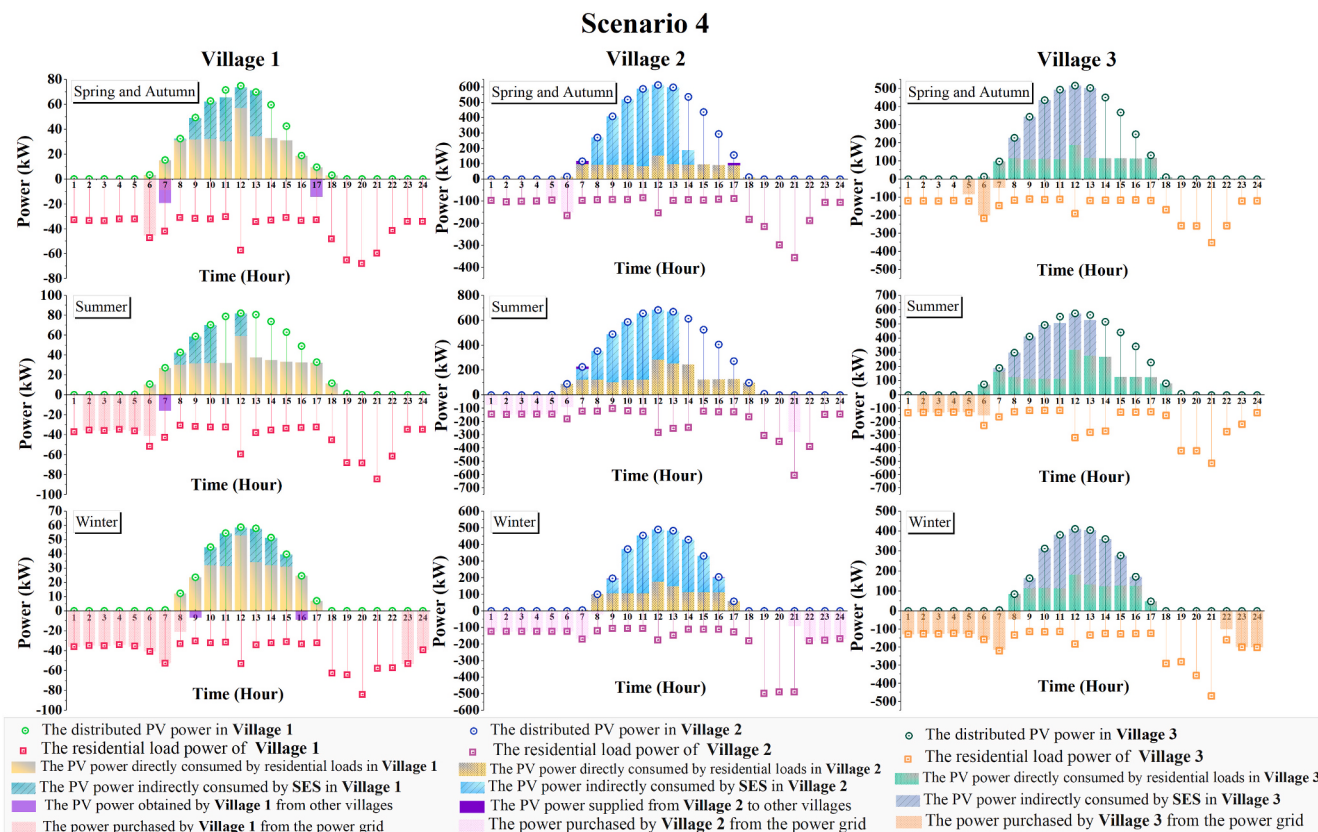


Fig. 24. The situation of PV-self consumption and self-sufficiency in different villages in Scenario 4.

Table 7

The results of PV self-consumption and self-sufficiency in different villages in Scenario 1.

Indicators	Mid-period: the 12-th year			Full life cycle
	Village 1	Village 2	Village 3	All villages
PV power (kW)	197,389	1,644,912	1,381,726	76,724,750
PV power directly consumed by residential loads (kW)	124,644	493,319	535,275	28,509,820
Proportion of self-generation and self-consumption (%)	63.15	29.99	38.74	37.16
Proportion of PV self-consumption (%)	63.15	29.99	38.74	37.16
Load power (kW)	362,067	1,420,104	1,513,438	82,955,389
Power purchased from the power grid (kW)	237,422	926,785	978,163	54,445,569
Proportion of purchasing power from the power grid (%)	65.57	65.26	64.63	65.63
Proportion of power self-sufficiency (%)	34.43	34.74	35.37	34.37

Table 8

The results of PV-self consumption and self-sufficiency in different villages in Scenario 2.

Indicators	Mid-period: the 12-th year			Full life cycle
	Village 1	Village 2	Village 3	All villages
PV power (kW)	197,389	1,644,912	1,381,726	76,724,750
PV power directly consumed by residential loads (kW)	124,644	493,319	535,275	28,509,820
PV power indirectly consumed by DES (kW)	36,512	817,300	547,106	34,074,088
Proportion of self-generation and self-consumption (%)	63.15	29.99	38.74	37.16
Proportion of DES consumption (%)	18.50	49.69	39.60	44.41
Proportion of PV self-consumption (%)	81.65	79.68	78.34	81.57
Load power (kW)	362,067	1,420,104	1,513,438	82,955,389
Power purchased from the power grid (kW)	197,312	109,484	431,057	20,371,481
Proportion of purchasing power from the power grid (%)	54.50	7.71	28.48	24.56
Proportion of power self-sufficiency (%)	45.50	92.29	71.52	75.44

Scenario 3 demonstrates enhanced system efficiency through different villages power complementarity and storage sharing. Specifically, the SES optimally utilizes surplus PV generation during peak production hours to charge the SES, while strategically discharging during peak consumption periods to meet load demand requirements. Comparative analysis reveals that the SES exhibits delayed and more distributed discharge patterns relative to Scenario 2. For instance, during spring/autumn typical days, the DES systems in Village 1 (Scenario 2) initiate discharge at 17:00, reaching the lower discharge limit by 22:00. In contrast, the SES (Scenario 3) maintains continuous discharge from 18:00 until 05:00 the following day, demonstrating significantly enhanced capacity utilization. Furthermore, the SOC profile in Scenario 3 shows improved stability and better alignment with the load demand

Table 9

The results of PV-self consumption and self-sufficiency in different villages in Scenario 3.

Indicators	Mid-period: the 12-th year			Full life cycle
	Village 1	Village 2	Village 3	All villages
PV power (kW)	197,389	1,644,912	1,381,726	76,724,750
PV power directly consumed by residential loads (kW)	124,644	493,319	535,275	28,509,820
PV power indirectly consumed by SES (kW)	42,672	902,320	600,723	35,351,462
Surplus PV power consumed by complementarity (kW)	0	8926	0	595,181
Proportion of self-generation and self-consumption (%)	63.15	29.99	38.74	37.16
Proportion of SES consumption (%)	21.62	54.86	43.48	46.08
Proportion of surplus PV power consumed by complementarity (%)	0.00	0.54	0.00	0.78
Proportion of PV self-consumption (%)	84.77	85.39	82.22	84.01
Load power (kW)	362,067	1,420,104	1,513,438	82,955,389
Power purchased from the power grid (kW)	61,470	289,539	282,460	18,498,926
Proportion of purchasing power from the power grid (%)	16.98	20.39	18.66	22.30
Proportion of power self-sufficiency (%)	83.02	79.61	81.34	77.70

Table 10

The results of PV-self consumption and self-sufficiency on typical days in different villages in Scenario 4.

Indicators	Mid-period: the 12-th year			Full life cycle
	Village 1	Village 2	Village 3	All villages
PV power (kW)	197,389	1,644,912	1,381,726	76,724,750
PV power directly consumed by residential loads (kW)	123,808	489,341	541,754	28,476,748
PV power indirectly consumed by SES (kW)	42,864	863,563	617,586	25,320,832
Surplus PV power consumed by complementarity (kW)	0	8949	0	267,112
Proportion of self-generation and self-consumption (%)	62.72	29.75	39.21	37.12
Proportion of SES consumption (%)	21.72	52.50	44.70	33.00
Proportion of surplus PV power consumed by complementarity (%)	0.00	0.54	0.00	0.35
Proportion of PV self-consumption (%)	84.44	82.79	83.91	85.03
Load power (kW)	362,067	1,420,104	1,513,438	82,955,389
Power purchased from the power grid (kW)	61,178	280,636	262,203	17,716,334
Proportion of purchasing power from the power grid (%)	16.90	19.76	17.33	21.36
Proportion of power self-sufficiency (%)	83.10	80.24	82.67	78.64

Table 11

The cost-income status for rural residents in different scenarios.

Indicators	Scenario 1	Scenario 2	Scenario 3	Scenario 4	
Cost	Initial investment of DPV (CNY)	6,840,400	6,840,400	6,840,400	6,840,400
	Average annual operation and maintenance costs of DPV (CNY/Year)	68,404	68,404	68,404	68,404
	Initial investment of ES (CNY)	/	5,425,177	5,231,750	4,991,810
	Average annual operation and maintenance costs of ES (CNY/Year)	/	162,755	156,953	149,754
	Replacement cost of ES (CNY)	/	8,137,766	7,847,625	7,487,715
	Average annual purchasing power from the grid (CNY/Year)	1,398,561	396,345	335,689	296,080
Income	Average annual grid-connected income of DPV (CNY/Year)	522,650	153,287	132,988	124,505
	Initial subsidy income of DPV (CNY)	392,000	392,000	392,000	392,000
	Total subsidy income of ES discharge (CNY)	/	1,970,629	2,036,041	2,100,957
	Residual value of fixed asset (CNY)	63,017	187,965	183,510	177,984
	Levelized annual cost per household (CNY/Year)	2517	3288	3205	3166

compared to Scenario 2.

In Scenario 4, the implementation of TOU price-based DR mechanisms enables rural residents to adjust their electricity consumption patterns in response to price signals, effectively reducing peak load demand while increasing off-peak consumption. This load-shifting strategy significantly alleviates operational pressure on the ES system,

resulting in smoother charge-discharge cycles.

5.4.3. Comparative analysis of PV self-consumption and self-sufficiency

The PV self-consumption and self-sufficiency for each village under different scenarios are shown in Fig. 21 to 24, and the results are shown in Tables 7–10.

Scenario 1: The annual PV self-consumption ratios for the three village areas are 63.15 %, 29.99 %, and 38.74 %, respectively, with an overall ratio of 37.16 % within the rural distribution network. This limited PV self-consumption necessitates grid integration for over half of the DPV power, leading to technical challenges such as grid current back-feeding, voltage overruns, harmonic pollution, and protection device failures, thereby compromising power quality. Additionally, accommodating extensive DPV integration requires costly upgrades to the rural distribution grid, increasing investment pressure. The power self-sufficiency proportions for the three villages are 34.43 %, 37.74 %, and 35.37 %, respectively, with an overall proportion of 34.37 %. This reliance on traditional thermal power generation exacerbates carbon emissions and environmental pollution.

Scenario 2: Following the configuration of DES systems in each of the three villages, the PV self-consumption ratios significantly improved to 81.64 %, 79.68 %, and 78.34 %, respectively, with the overall PV self-consumption ratio rising to 81.57 %. Concurrently, the proportion of power self-sufficiency markedly increased to 45.50 %, 92.29 %, and 71.52 % for Village 1 to Village 3, respectively, resulting in an overall promotion to 75.44 %. This demonstrates the substantial efficacy of ES systems in PV self-consumption and self-sufficiency. By significantly boosting the PV self-consumption and reducing reliance on the power grid electricity, the ES systems play a pivotal role in improving energy utilization efficiency and mitigating environmental pollution.

Scenario 3: The adoption of SES further augments PV self-consumption and self-sufficiency. The PV self-consumption ratios for the villages are 84.76 %, 85.39 %, and 82.22 %, respectively, with an overall ratio of 84.01 % within the rural distribution network. The power self-sufficiency proportion increases to 77.70 %, representing a 2.44 % increase in PV self-consumption and a 2.26 % increase in self-sufficiency compared to Scenario 2.

Scenario 4: Integrating TOU price-based DR with SES yields further improvements. The PV self-consumption ratios for the villages rise to 84.44 %, 82.79 %, and 83.91 %, respectively, with an overall ratio of 85.03 %. The power self-sufficiency proportions increase to 78.67 %, reflecting a 3.46 % increase in PV local consumption and a 3.20 %

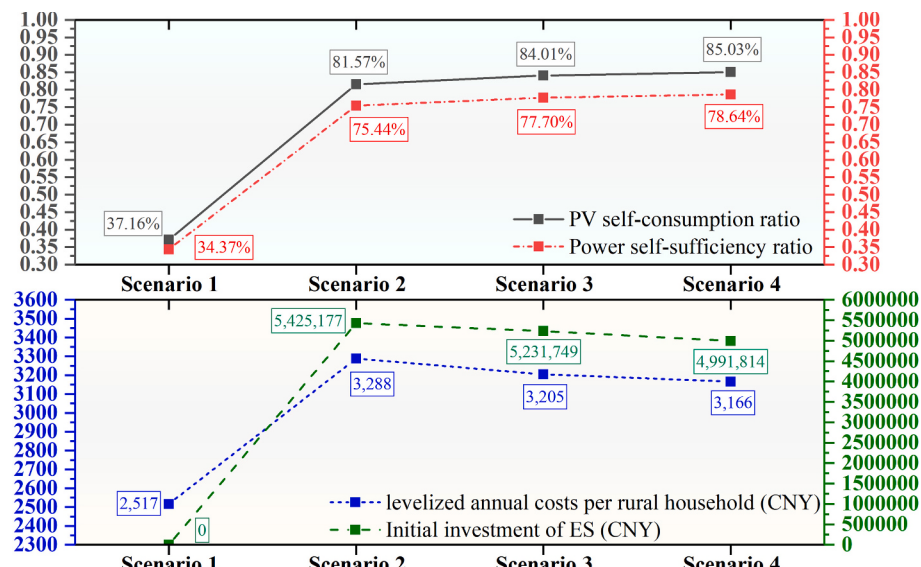


Fig. 25. The changing trends of key indicators in different scenarios.

increase in self-sufficiency compared to Scenario 2.

Comparative analysis across scenarios reveals that ES systems significantly enhance PV self-consumption and reduce grid reliance. SES outperforms distributed storage in these metrics, while DR mechanisms further optimize power resource allocation, achieving superior energy efficiency.

5.4.4. Comparative analysis of cost-income for rural residents

The cost-income status for rural residents in different scenarios are shown in the Table 11:

By comparing and analyzing the cost-income indicators under the four scenarios, it can be seen that Scenario 1 (without ES configuration) is more advantageous in terms of economic benefits. However, the grid integration of large-scale PV power generation affects the power quality of the power system. In order to ensure the safe and reliable operation of the power system, the power grid has to increase the cost of distribution network upgrading and transformation, and the cost of the system external increases, and Scenario 1 is unfriendly to the safe and economic operation of the power system.

Fig. 25 presents the changing trends of key indicators in different scenarios. Scenarios 1, 2, 3, and 4 exhibit progressively enhanced PV local consumption ratios at 37.16 %, 81.57 %, 84.01 %, and 85.03 %, respectively, with corresponding power self-sufficiency ratios of 34.37 %, 75.44 %, 77.70 %, and 78.64 %. However, in scenarios with ES configuration, the initial ES investments show a decreasing trend from 5,425,177 CNY to 5,231,749 CNY and 4,991,814 CNY, and the levelized annual costs per rural household decline from 3288 CNY to 3205 CNY and 3166 CNY. This demonstrates that the configurations of SES achieve enhanced PV self-consumption and reduced power grid dependence while achieving lower investment and operational costs. The implementation of DR mechanisms further optimizes both SES investments and the levelized annual costs for rural households.

5.5. Suggestions for enhancing the PV self-consumption and economic efficiency of rural distribution networks

Rural multi-DPV clusters combined with SES systems face the challenge of high costs due to significant initial investment in storage infrastructure. However, integrating SES with multi-DPV clusters can substantially enhance the self-consumption of rural power distribution networks, mitigate the impact of PV integration, and ensure safe, reliable, and cost-effective operation, while offering notable environmental and social benefits. Thus, improving local PV utilization, optimizing system economics, and accelerating capital recovery are essential. The following recommendations are proposed:

- (1) Enhance the cost compensation mechanism for DPV and ES systems: Governments should introduce targeted subsidies or incentive policies to reduce both investment and operational costs, thereby attracting greater third-party investment.
- (2) Implement the time-of-use electricity pricing policy for residents, guiding electricity consumption behavior through price signals, to achieve the dual goals of local consumption of PV power generation and reduction of electricity costs.
- (3) Explore diverse market trading models for distributed power generation: For instance, aggregated multi-DPV clusters could participate in provincial electricity markets, enabling cross-regional electricity sales. Alternatively, aggregating distributed generation, flexible loads, and ES into a virtual power plant can create a balanced unit to participate in grid regulation, alleviating system regulation pressures while generating regulatory benefits.
- (4) Accelerate smart terminal construction and enhance load response capability: Flexible load resources such as electric vehicle charging stations, water heaters, and air conditioners in rural homes can be managed using intelligent control

technologies. This would enable “load-source synchronization,” adjusting the load power curve based on PV output, thereby saving residents’ electricity costs and increasing local PV consumption.

- (5) Strengthen the construction and upgrading of rural distribution networks: A comprehensive enhancement of rural electrification is necessary, focusing on building distribution grids capable of supporting large-scale distributed renewable energy integration, thus facilitating the large-scale development and efficient use of renewable energy.

6. Conclusions

Addressing the practical challenge of integrating DPV generation into the grid while ensuring its safe and stable operation, this paper explores the complementarity between multi-DPV clusters output and residential electricity consumption across various villages in rural distribution networks. To enhance PV self-consumption, a cooperative operation strategy for multi-DPV clusters with SES is proposed. A two-stage optimization model for SES configuration is developed, with the goal of strengthening the PV self-consumption and self-sufficiency of rural distribution networks and improving the economic benefits for rural residents. The results indicate that:

- (1) The ES system significantly enhances PV self-consumption and self-sufficiency. Compared to the non-ES scenario, the configuration of ES increased the PV self-consumption rate by 44.41 %, while increasing self-sufficiency by 41.07 %.
- (2) Compared to DES, SES demonstrates superior performance in enhancing self-consumption and self-sufficiency and cost reduction. Relative to the DES configuration, SES improved PV self-consumption by 2.44 % and 3.46 %, increased self-sufficiency by 2.26 % and 3.20 %, and lowered levelized annual costs by 2.54 % and 3.72 %.
- (3) Under the combined influence of SES and DR, PV self-consumption and self-sufficiency is further optimized, leading to a 1.18 % reduction in the levelized annual costs for rural residents.

Overall, the configuration of SES and the adoption of a DR mechanism offer an effective approach to enhancing the PV self-consumption and self-sufficiency of rural distribution networks while reducing residential costs. The findings of this study provide valuable insights into the collaborative operation of multi-DPV clusters and SES in rural areas, contributing to the sustainable development of rural DPV systems. However, this study has certain limitations, particularly regarding the cost and benefit-sharing mechanisms of DPV clusters and SES systems, which require further exploration. Future research will address this issue to enhance the model’s practicality and economic viability.

CRediT authorship contribution statement

Keyi Kang: Visualization, Validation, Supervision, Methodology, Investigation. **Heping Jia:** Writing – review & editing, Writing – original draft, Software. **Hongxun Hui:** Formal analysis, Data curation. **Dunnan Liu:** Conceptualization.

Declaration of competing interest

The authors declare that they have no known competing financial interests or personal relationships that could have appeared to influence the work reported in this paper.

Acknowledgements

The research is partially supported by the National Key Research and

Development Program of China (2022YFB2403000).

Data availability

Data will be made available on request.

References

- [1] Chen S, Heilscher G. Integration of distributed PV into smart grids: a comprehensive analysis for Germany. *Energ Strat Rev* 2024:55. <https://doi.org/10.1016/j.esr.2024.101525>.
- [2] National Energy Administration. Policy interpretation of the management measures for the development and construction of distributed photovoltaic power generation. <https://www.nea.gov.cn/20250123/d38e5436b4d04159863ddbc10a6ede10/c.html>. 2025. Accessed 1 February 2025.
- [3] National Energy Administration. Transcript of the press conference for the first quarter of 2025 by the National Energy Administration. <https://www.nea.gov.cn/20250123/544b9af2b6aa4590a60945e81e0d8ee1/c.html>. 2025. Accessed 1 February 2025.
- [4] National Energy Administration. Notice on Further Implementing the "Thousand Households Bathing in Sunshine" Initiative Issued by the General Office of the National Energy Administration. https://www.gov.cn/zhengce/zhengceku/2025/3/content_7015273.htm. 2025. Accessed 1 May 2025.
- [5] Changjiang Business Daily. Household photovoltaics face the growing pains! Where is the road to breaking through in 2025? <http://www.changjiangtimes.com/2025/01/643927.html>. 2025. Accessed 1 February 2025.
- [6] Zhang W, Chen Y, Xie R, Xu Y. A multi-timescale and chance-constrained energy dispatching strategy of integrated heat-power community with shared hybrid energy storage. *J Energy Storage* 2024:97. <https://doi.org/10.1016/j.est.2024.112505>.
- [7] Han O, Ding T, Zhang X, Mu C, He X, Zhang H, et al. A shared energy storage business model for data center clusters considering renewable energy uncertainties. *Renew Energy* 2023;202:1273–90. <https://doi.org/10.1016/j.renene.2022.12.013>.
- [8] Sun B, Jing R, Zeng Y, Wei W, Jin X, Huang B. Three-side coordinated dispatching method for intelligent distribution network considering dynamic capacity division of shared energy storage system. *J Energy Storage* 2024:81. <https://doi.org/10.1016/j.est.2023.110406>.
- [9] Tercan SM, Demirci A, Gokalp E, Cali U. Maximizing self-consumption rates and power quality towards two-stage evaluation for solar energy and shared energy storage empowered microgrids. *J Energy Storage* 2022:51. <https://doi.org/10.1016/j.est.2022.104561>.
- [10] Zabihinia Gerdroobari Y, Khorasany M, Razzaghi R, Heidari R. Management of prosumers using dynamic export limits and shared community energy storage. *Appl Energy* 2024:355. <https://doi.org/10.1016/j.apenergy.2023.122222>.
- [11] Chen X, Liu Z, Wang P, Li B, Liu R, Zhang L, et al. Multi-objective optimization of battery capacity of grid-connected PV-BESS system in hybrid building energy sharing community considering time-of-use tariff. *Appl Energy* 2023:350. <https://doi.org/10.1016/j.apenergy.2023.121727>.
- [12] Liu Y, Liu D, Kang K, Wang G, Rong Y, Wang W, et al. Research on two-stage energy storage optimization configurations of rural distributed photovoltaic clusters considering the local consumption of new energy. *Energies* 2024;17:6272. <https://doi.org/10.3390/en17246272>.
- [13] Cao W, Xiao J-W, Cui S-C, Liu X-K. An efficient and economical storage and energy sharing model for multiple multi-energy microgrids. *Energy* 2022:244. <https://doi.org/10.1016/j.energy.2022.123124>.
- [14] Fachrizal R, Shepero M, Åberg M, Munkhammar J. Optimal PV-EV sizing at solar powered workplace charging stations with smart charging schemes considering self-consumption and self-sufficiency balance. *Appl Energy* 2022:307. <https://doi.org/10.1016/j.apenergy.2021.118139>.
- [15] Ramos S, Roque LAC, Gomes A, Soares J, Rolle JC, Vale Z. Multi-objective model for residential energy management in context of individual self-consumption. *Math Comput Simul* 2025;231:120–7. <https://doi.org/10.1016/j.matcom.2024.11.017>.
- [16] Zare Ghaleh Seyyedi A, Gitizadeh M, Fakhrooeian M, Jabareh Nasero M. Achieving the goals of energy arbitrage, peak-shaving, and PV self-consumption using PV-BTM BESS microgrids coupled with a distribution network. *J Energy Storage* 2025; 112. <https://doi.org/10.1016/j.est.2025.115479>.
- [17] Zhan S, Dong B, Chong A. Improving energy flexibility and PV self-consumption for a tropical net zero energy office building. *Energ Build* 2023:278. <https://doi.org/10.1016/j.enbuild.2022.112606>.
- [18] Allouhi A. Solar PV integration in commercial buildings for self-consumption based on life-cycle economic/environmental multi-objective optimization. *J Clean Prod* 2020:270. <https://doi.org/10.1016/j.jclepro.2020.122375>.
- [19] Jiang X, Tang B, Yu G, Hu P, Xia X, Xu L. Coordination and optimization method of park-level energy storage and electricity Price for local accommodation of renewable energy. *Automation Elect Power Syst* 2022:46. <https://doi.org/10.7500/AEPS20210601004>.
- [20] Shao Z, Zhao Q, Zhang Y. Source side and load side coordinated configuration optimization for stand-alone Micro-grid. *Power Syst Technol* 2021:45. <https://doi.org/10.13355/j.1000-3673.pst.2020.2028>.
- [21] Argyrou MC, Marouchos CC, Kalogirou SA, Christodoulides P. Analytical approach for maximizing self-consumption of nearly zero energy buildings- case study. *Energy Convers Manag* 2021:246. <https://doi.org/10.1016/j.energy.2021.121744>.
- [22] Ahmadiahangar R, Karami H, Husev O, Blinov A, Rosin A, Jonaitis A, et al. Analytical approach for maximizing self-consumption of nearly zero energy buildings- case study: Baltic region. *Energy* 2022:238. <https://doi.org/10.1016/j.energy.2021.121744>.
- [23] Mulleriyawage UGK, Wang P, Rui T, Zhang K, Hu C, Shen WX. Prosumer-centric demand side management for minimizing electricity bills in a DC residential PV-battery system: an Australian household case study. *Renew Energy* 2023;205: 800–12. <https://doi.org/10.1016/j.renene.2023.01.029>.
- [24] Abdalla MAA, Min W, Bing W, Ishag AM, Saleh B. Double-layer home energy management strategy for increasing PV self-consumption and cost reduction through appliances scheduling, EV, and storage. *Energy Rep* 2023;10:3494–518. <https://doi.org/10.1016/j.egyr.2023.10.019>.
- [25] Luo S, Chen C, Qiu W, Ma J, Yang L, Lin Z. Bi-layer optimal planning of rural distribution network based on KKT condition and big-M method. *Energy Rep* 2021; 7. <https://doi.org/10.1016/j.egyr.2021.09.206>.
- [26] Sun T, Shan M, Rong X, Yang X. Estimating the spatial distribution of solar photovoltaic power generation potential on different types of rural rooftops using a deep learning network applied to satellite images. *Appl Energy* 2022:315. <https://doi.org/10.1016/j.apenergy.2022.119025>.
- [27] Wang W, Kang K, Sun G, Xiao L. Configuration optimization of energy storage and economic improvement for household photovoltaic system considering multiple scenarios. *J Energy Storage* 2023:67. <https://doi.org/10.1016/j.est.2023.107631>.
- [28] Wang W, Li C, He Y, Bai H, Jia K, Kong Z. Enhancement of household photovoltaic consumption potential in village microgrid considering electric vehicles scheduling and energy storage system configuration. *Energy* 2024:311. <https://doi.org/10.1016/j.energy.2024.133330>.
- [29] Wang H, Liao Y, Zhang J, Cai Z, Zhao Y, Wang W. Optimization of shared energy storage configuration for village-level photovoltaic systems considering vehicle charging management. *Energy* 2024:311. <https://doi.org/10.1016/j.energy.2024.133373>.
- [30] Li L, Cao X, Zhang S. Shared energy storage system for prosumers in a community: investment decision, economic operation, and benefits allocation under a cost-effective way. *J Energy Storage* 2022:50. <https://doi.org/10.1016/j.est.2022.104710>.
- [31] Kang H, Jung S, Kim H, Hong J, Jeoung J, Hong T. Multi-objective sizing and real-time scheduling of battery energy storage in energy-sharing community based on reinforcement learning. *Renew Sust Energ Rev* 2023:185. <https://doi.org/10.1016/j.rser.2023.113655>.
- [32] Li J, Zhu Y, Xiao Y, Lan X. Optimized configuration and operation model and economic analysis of shared energy storage based on master-slave game considering load characteristics of PV communities. *J Energy Storage* 2024:76. <https://doi.org/10.1016/j.est.2023.109841>.
- [33] Chang H-C, Ghaddar B, Nathwani J. Shared community energy storage allocation and optimization. *Appl Energy* 2022:318. <https://doi.org/10.1016/j.apenergy.2022.119160>.
- [34] Ma M, Huang H, Song X, Peña-Mora F, Zhang Z, Chen J. Optimal sizing and operations of shared energy storage systems in distribution networks: a bi-level programming approach. *Appl Energy* 2022:307. <https://doi.org/10.1016/j.apenergy.2021.118170>.
- [35] Yang H, Yang Z, Gong M, Tang K, Shen Y, Zhang D. Commercial operation mode of shared energy storage system considering power transaction satisfaction of renewable energy power plants. *J Energy Storage* 2025:105. <https://doi.org/10.1016/j.est.2024.114738>.
- [36] Cao Z, Zhang M, Zhai C, Wang Y. Scheduling optimization of shared energy storage station in industrial park based on reputation factor. *Energ Build* 2023:299. <https://doi.org/10.1016/j.enbuild.2023.113596>.
- [37] Gülmез B. GA-attention-fuzzy-stock-net: an optimized neuro-fuzzy system for stock market price prediction with genetic algorithm and attention mechanism. *Heliyon* 2025;11. <https://doi.org/10.1016/j.heliyon.2025.e42393>.
- [38] Xu X, Guan L, Wang Z, Yao R, Guan X. A double-layer forecasting model for PV power forecasting based on GRU-informer-SVR and blending ensemble learning framework. *Appl Soft Comput* 2025:172. <https://doi.org/10.1016/j.asoc.2025.112768>.
- [39] Wang C, Liu Y, Zhang Y, Xi L, Zhao Z, et al. Strategy for optimizing the bidirectional time-of-use electricity price in multi-microgrids coupled with multilevel games. *Energy* 2025:323. <https://doi.org/10.1016/j.energy.2025.135731>.
- [40] Ouyang D, Weng J, Chen M, Wang J, Wang Z. Sensitivities of lithium-ion batteries with different capacities to overcharge/over-discharge. *J Energy Storage* 2022:52. <https://doi.org/10.1016/j.est.2022.104997>.
- [41] Gao Y, Cai Y, Liu C. Annual operating characteristics analysis of photovoltaic-energy storage microgrid based on retired lithium iron phosphate batteries. *J Energy Storage* 2022:45. <https://doi.org/10.1016/j.est.2021.103769>.
- [42] Chreim B, Esseghir M, Merghem-Boulahia L. SPLANDID — Optimal sizing, placement, and management of centralized and distributed shared battery energy storage systems in residential communities: application to smart grids. *Sustain Cities Soc* 2024:113. <https://doi.org/10.1016/j.scs.2024.105694>.
- [43] National Bureau of Statistics. China Statistical Yearbook. <https://www.stats.gov.cn/sj/ndsj/>. 2025. Accessed 23 March 2025.
- [44] The Standardization Administration of the People's Republic of China. Guide for choice power transformers, GB/T 17468–2019. 2025. p. 3–25 (In Chinese).
- [45] National Power Energy Storage Standardization Technical Committee (SAC/TC 550). General technical requirements for electrochemical energy storage system in power system, GB/T 36558–2018. 2025. p. 1–31 [In Chinese].